Christie, D.M., Pedersen, R.B., Miller, D.J., et al., 2001
Proceedings of the Ocean Drilling Program, Initial Reports Volume 187

6. SITE 1155[1]

Shipboard Scientific Party[2]

PRINCIPAL RESULTS

Site 1155 is located in Segment B5 on ~25-Ma seafloor, west of the locus of the residual depth anomaly. In this region, the fracture zones bounding Segment B5 are only ~55 km apart. Site 1155 is placed near midsegment in normal abyssal hill terrain. This is one of several sites whose purpose is to establish the temporal variability of the mantle source and of magmatic processes beneath this segment.

Hole 1155A was spudded in ~4986 m water depth and was washed through ~177 m of sediment, from which a wash core containing siliceous pelagic clay overlying calcareous clay was recovered. We drilled 26.2 m into volcanic basement, recovering 2.3 m of pillow basalt from two lithologic units. Both the upper, sparsely to moderately plagioclase-olivine phyric pillow basalt (Unit 1) and the lower, aphyric basalt (Unit 2) have undergone low-temperature alteration, replacing olivine and groundmass material with clay and Fe oxyhydroxides. Because hole conditions deteriorated rapidly in Unit 2 and most pieces recovered from that unit are bounded by weathered (predrilling) fracture surfaces, we conclude that we drilled into unconsolidated talus.

Hole 1155B was spudded 200 m west of Hole 1155A and was washed through ~148 m of sediment, recovering 38 cm of dark brown clay in a single wash core. Volcanic basement was encountered 30 m shallower than in Hole 1155A, and 18.2 m of moderately plagioclase-olivine phyric pillow basalt from a single lithologic unit was recovered. Micritic limestone is common, both as interpillow fill and as fracture fillings. The basalt has undergone pervasive low-temperature alteration to clay and Fe oxyhydroxides, with the degree of alteration decreasing downhole. Glass rims are invariably altered along fractures to palagonite, and microtextures attributed to biodegradation are common.

Two handpicked glasses, a plagioclase separate, and seven whole-rock powders were analyzed on board. The Hole 1155B glass is quite primi-

[1]Examples of how to reference the whole or part of this volume.
[2]Shipboard Scientific Party addresses.

Ms 187IR-106

tive, with 9.3 wt% MgO, whereas the Hole 1155A glass is moderately evolved, with 7.8 wt% MgO. As at the previous sites, the whole rocks have significantly less MgO than their associated glasses, and this difference does not appear to be attributable to crystal fractionation or crystal sorting. Nevertheless, the whole rocks appear to lie on a coherent low-pressure trend that is offset from the glass compositions to lower CaO, Al_2O_3, and Ni, consistent with the inclusion of olivine and plagioclase phenocrysts in the whole-rock powder but not in the glass separates.

Relative to 0- to 5-Ma glasses from Segment B5, Site 1155 glasses have distinctly higher TiO_2, Fe_2O_3, Zr, and Y and lower Al_2O_3 for a given MgO content, with relatively constant Na_2O and CaO/Al_2O_3. Together, these compositional differences seem more likely to reflect temporal variations in mantle composition than variations in melting conditions.

The Zr/Ba systematics of Site 1155 suggest that the mantle source beneath this area at the time of eruption was in some way mixed, with both Indian- and Pacific-type components being present and maintaining their separate identities. The Unit 2 glass and the Unit 1 whole rock from Hole 1155A were derived from a Transitional-Pacific–type source, whereas the Unit 2 whole rock and all the Hole 1155B samples are of Indian type, comparable to some axial Segment B5 lavas.

OPERATIONS

Transit to Site 1155

The 149-nmi transit to Site 1155 took just over 16 hr at an average speed of 9.1 kt. The reduced transit speed was a result of a course directly into a swell and against the current. At 1345 hr on 5 December, we began a single-channel seismic (SCS) and 3.5-kHz survey. We interpreted these data to indicate that the sediment cover at this site was ~200 m thick.

Hole 1155A

When the survey was concluded, the vessel came about and slowly approached our prospectus site location. We deployed a positioning beacon on Global Positioning System (GPS) coordinates at 1454 hr on 5 December. Precision depth recorder (PDR) water depth was 4986.4 m below the rig floor (4975.4 m below sea level). The nine-collar bottomhole assembly employed on previous sites was made up with a new C-7 four-cone rotary bit.

We began washing down through the sediment column at Hole 1155A at 0215 hr on 6 December and encountered basement at 177.3 meters below seafloor (mbsf). We rotary cored from 177.3 to 203.5 mbsf with an average recovery of 9% (Table T1). In an effort to increase recovery we retrieved core barrels after an average cored interval of 4.5 m. Fluorescent microsphere tracers were deployed in the core catchers of Cores 187-1155A-2R and 7R. After we recovered Core 7R, indications from drilling parameters (stalling top drive and high torque) suggested poor hole conditions. Hoping for better recovery, we decided to terminate this hole, offset 200 m west, and initiate a second hole. We determined the direction and magnitude of the offset based on a review of the precruise seismic data, as well as the SCS record obtained during our survey. The seismic data indicated slightly thinner sediment cover over

T1. Coring summary, Site 1155, p. 39.

a local basement high, and our intuition suggested there might be less rubble updip. The drill string cleared the seafloor at 0330 hr on 7 December.

Hole 1155B

At 0500 on 7 December, we began washing down to basement and started coring at 147.9 mbsf after we encountered a hard contact. We advanced Hole 1155B from 147.9 to 193.0 mbsf (Cores 187-1155B-2R to 9R) and averaged 50% recovery while coring 4.6- to 5-m intervals. We deployed microsphere tracers on Cores 187-1155B-2R and 9R. When we tried to recover Core 187-1155B-10R, the core barrel arrived on deck empty, with the core catcher fingers missing. As we had retrieved sufficient material to meet our objectives, rather than attempt to clean the hole, we decided to terminate operations and move to our next site. The bit cleared the seafloor at 2130 hr on 8 December, and the vessel was under way by 0700 hr on 9 December.

IGNEOUS PETROLOGY

Introduction

Holes 1155A and 1155B were rotary cored into igneous basement from 177.3 to 203.5 and 147.9 to 193.9 mbsf, respectively. Hole 1155A was drilled (Sections 187-1155A-2R-1 through 7R-1) 26.2 m into basement, resulting in 2.34 m of recovered core (equal to 8.93% recovery). Lavas from this hole have been assigned to two units. Unit 1 consists of a sparsely to moderately plagioclase ± olivine phyric basalt, present in Sections 187-1155A-2R-1 through 4R-1; Unit 2 is an aphyric basalt, present in Sections 187-1155A-5R-1 through 7R-1. Unit 2 is dominated by pebble- and cobble-sized fragments with weathered, not drilled, outer surfaces. We interpret Unit 1 as a pillow lava overlying the loose basalt talus of Unit 2.

Hole 1155B was drilled (Sections 187-1155B-2R-1 through 10R-1) 46 m into basement, resulting in 18.18 m of recovered core (equal to 39.52% recovery). Section 187-1155B-10R-1 was drilled 9.6 m into basement with no recovery because of a broken core catcher. Prior to this section, recovery was 49.95%. Lavas from this hole were assigned to a single lithologic unit of moderately plagioclase ± olivine phyric basalt. We interpret this hole as having sampled an intact pillow lava sequence, based on its uniform lithology and the high percentage of pieces with glassy rinds and chilled margins (42.26%: 112 of 265 pieces). Light pink micritic limestone is present in interpillow spaces attached to glassy margins (Fig. F1) and as infill along fractures perpendicular to glassy margins (Sections 187-1155B-6R-1 through 6R-4; Sections 187-1155B-8R-1 through 9R-1) (e.g., Fig. F2).

Hole 1155A

Unit 1

This unit comprises a medium gray, sparsely to moderately plagioclase-olivine phyric basalt that is slightly altered overall (see "Alteration," p. 5). The basalt contains <1% small (<0.5 mm in diameter), rounded vesicles that are typically lined with smectite and have calcite filling the interior (Fig. F3). The unit contains 3% glomerocrysts of pla-

F1. Micritic limestone infilling a fracture and interpillow space, p. 14.

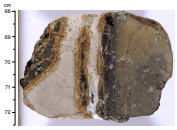

F2. A sparry calcite vein and micritic limestone infilling a fracture running perpendicular to the chilled margin, p. 15.

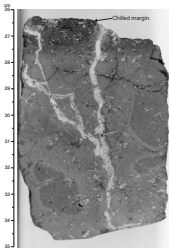

F3. Vesicle lined with smectite and filled with calcite, p. 16.

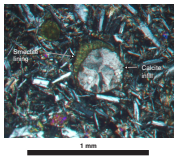

gioclase ± olivine, with plagioclase as the more abundant phase. Plagioclase is prismatic to tabular, as large as 5 mm in size, and commonly twinned. Olivine is equant and as large as 3 mm in size. Subrounded plagioclase—usually with corroded, probably resorbed, rims surrounding uncorroded euhedral cores—is present.

As seen in thin section, the microcrystalline groundmass texture is intersertal with plumose quench textures. The groundmass consists of 45% clinopyroxene (plumose quench growths), 40% prismatic to tabular to microlitic plagioclase with some acicular overgrowths, 1% equant olivine, and 14% mesostasis.

Unit 2

This unit consists predominantly of a slightly to moderately altered (see "Alteration," p. 5), medium gray aphyric basalt. Several pieces of moderately plagioclase-olivine phyric basalt were also recovered, but whether these are in situ or fell into the hole from Unit 1 above is unclear. The aphyric basalt contains <1% small (<0.5 mm in diameter), spherical vesicles that are filled with smectite. Very rare anhedral to subhedral plagioclase (up to 2 mm) and anhedral olivine (up to 0.6 mm) are present in <1% of the unit. The few phenocrysts present usually form glomerocrysts of plagioclase ± olivine. The plagioclase is typically twinned and displays oscillatory zoning. Some of the plagioclase is sieve textured with rounded to oval holes, probably due to resorption (Fig. F4). A few pieces from this unit (e.g., Section 187-1155A-6R-1 [Piece 4]) display a typical pillow margin sequence grading from glass rind through a spherulitic band to a more crystalline interior.

The microcrystalline groundmass texture is intersertal (Fig. F4). Lath-like plagioclase and elongate clinopyroxene are present in equal proportions and account for ~85% of the groundmass. The remaining 15% of the groundmass consists of ~2% equant olivine and ~13% glass with cryptocrystalline quench phases; ~70% of each has been altered to Fe oxyhydroxide and palagonite, respectively.

The outsides of most pieces from this unit are fracture surfaces coated by clay and/or calcareous sediment with Mn oxide spots, typically <1 mm in size.

Hole 1155B

Unit 1

Unit 1 is a buff (where weathered) to medium gray (where fresh), moderately plagioclase-olivine phyric basalt that ranges from highly altered near the top of the hole to slightly altered at the bottom (see "Alteration," p. 5). Small (<0.5 mm in diameter), spherical vesicles are rare (<0.5% throughout the unit), and some are filled with clay. Subhedral prismatic to tabular plagioclase phenocrysts as long as 7 mm constitute 5% of the basalt. In some cases they are sieve textured (~15%), probably resorbed, with oval holes (Fig. F5) elongate parallel to fracture and cleavage planes. Subrounded plagioclase with corroded, probably resorbed, rims around euhedral uncorroded cores is also present. In most cases plagioclase is twinned, and some crystals display oscillatory zoning. Cr spinel inclusions are rare in plagioclase phenocrysts (Figs. F6, F7). Equant, subhedral olivine phenocrysts as large as 3 mm make up ~1%–2% of the basalt. Of the olivine phenocrysts, 10%–20% are partially to entirely altered to iddingsite. Glomerocrysts of plagioclase ± olivine are common. Both plagioclase phenocrysts and microphenocrysts

F4. Plagioclase phenocryst rounded by resorption, p. 17.

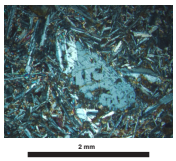

F5. Sieve texture in the core of a plagioclase phenocryst, p. 18.

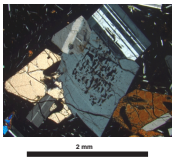

F6. A Cr spinel included in a plagioclase phenocryst, p. 19.

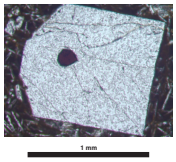

F7. Cr spinel included near the edge of a plagioclase phenocryst, p. 20.

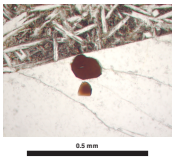

crysts are flow aligned near chilled margins in several pieces (e.g., Sections 187-1155B-2R-1 [Piece 9] and 5R-1 [Piece 5]; Fig. F8).

As seen in thin section, the microcrystalline groundmass texture is intersertal (Fig. F7). Plagioclase constitutes 45% of the groundmass, displaying acicular to lath-like quench morphologies. Equant olivine and opaque minerals make up 2% of the groundmass; the olivine is commonly altered to iddingsite. The remaining ~53% is mesostasis, including clinopyroxene quench textures and altered glass.

More than 40% of the pieces in this unit have glassy rinds and chilled margins. Many of these margins show transitions from fresh glass to spherulitic glass to coalesced spherulites (Fig. F9) to more crystalline interiors. Piece 11 in Section 187-1155B-8R-2 is cobble sized and consists of micritic limestone surrounding three ellipsoids of glass and palagonite pillow buds (3–3.5 cm across). The glassy margins of Pieces 1 and 13 are unusual in that they appear to have been folded back into the pillow lava (i.e., fingers of glass + palagonite + micritic limestone protrude into the more crystallized interior). These features may be a result of an eruption of pillow lavas into a slurry of calcareous ooze. However, this same sediment also fills fractures (with no chilled or glassy margin) (Fig. F2) and interpillow spaces. This suggests that some or all of the sediment may have formed after eruption and, through time, filtered into the pillow lava pile, perhaps with one or more significant time breaks.

F8. Plagioclase phenocryst abutting a calcite vein, p. 21.

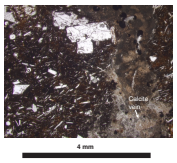

F9. A quench zone grading from fresh glass to spherulitic glass to coalesced spherulites, p. 22.

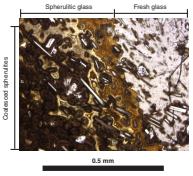

ALTERATION

Hole 1155A

Basalt recovered from Hole 1155A is slightly to moderately altered by low-temperature alteration. However, a few pieces are highly altered (e.g., Section 187-1155A-5R-1 [Piece 2]). The degree of alteration varies from piece to piece and within pieces. In hand specimen, basalt from Unit 1 (Sections 187-1155A-2R-1 through 4R-1) appears fresher than basalt from Unit 2 (Sections 187-1155A-5R-1 through 7R-1). Some basalt fragments are entirely bounded by buff weathered, roughly planar fracture surfaces (e.g., Section 187-1155A-7R-1 [Piece 6]), suggesting that they are blocky fragments from a talus deposit.

Fractures occur predominantly as exterior faces of pieces and are partially (40%–60%) coated with patchy encrustations of Mn oxide and, in some places, calcite. Fractures cutting across pieces are rare. Alteration halos extend from a few millimeters to 2 cm into pieces. In the most altered pieces, halos are subparallel to the piece margins, but in less altered pieces halo widths can be variable due to the irregular nature of the alteration front. As described for Sites 1153 and 1154, phenocrysts within the alteration halos are not visible on the cut surface in hand specimen but can be seen under the binocular microscope. Within the alteration halos, olivine is replaced by Fe oxyhydroxide where strongly altered and/or by a yellow-green clay (smectite?) where less altered (20%–60%). Olivine is mostly unaffected by alteration in the fresher piece interiors. Plagioclase phenocrysts are fresh throughout. Thin-section inspection of the groundmass confirms that replacement of olivine and clinopyroxene by Fe oxyhydroxide and smectite is lowest (~1%) in the fresher interiors of pieces and highest (~10%–15%) within the alteration halos. Vesicles are variably filled by cryptocrystalline silica, smectite, and Fe oxyhydroxide or by smectite and calcite; in the latter case,

calcite forms the center of the vesicle filling, suggesting that calcite precipitation occurred after smectite (Fig. F10A, F10B).

Hole 1155B

Low-temperature alteration is pervasive throughout Hole 1155B, with recovered basalt pieces ranging from highly to slightly altered. The overall degree of alteration decreases downhole from highly to moderately altered in Sections 187-1155B-2R-1 through 6R-4 to moderately to slightly altered in Sections 187-1155B-7R-1 through 9R-4. Alteration is strongest around fractures and glassy pillow margins and is clearly visible as oxidation halos as wide as 3 cm (Fig. F11). Altered fractures form two roughly orthogonal sets that are oriented perpendicular (1 mm to 1 cm wide) and parallel (<1–3 mm) to the chilled margins (Figs. F11, F12). Fracture densities are highest within several centimeters of the chilled margins, because in this area the fractures commonly form anastomosing networks. They are mainly filled with micritic calcite or sparry calcite; the gradation from micritic to sparry calcite can be seen in thin section. Additionally, sharp contacts between micritic calcite and sparry calcite growing perpendicular to the fracture walls are present in some specimens (Fig. F13).

Mn oxide is commonly associated with calcite, covering the inner walls of fractures (Fig. F12), or occurring as small (<0.2 mm) spots or clusters (0.5 mm) within the calcite veins (Fig. F14). Minute Mn oxide veins <0.1 mm wide commonly dissect even apparently fresh groundmass. In some places, several layers of milky white calcite are separated by thin dark layers of Mn oxide, indicating that the carbonate built up over several episodes, possibly within an opening fracture. Iron-stained silica veins occur exclusively within or near palagonitized pillow margins, reaching up to 4 cm into the pillows; beyond this point, the vein filling abruptly changes to calcite. Thin section inspection of calcite veins, however, reveals a more complex picture with linings of aragonite and silica ± Mn oxides at fracture edges (Fig. F15). One such vein taken near a glassy margin, analyzed by shipboard X-ray diffraction, consists of smectite and quartz; this underlines the complex interplay of fluid migration at the interface of crystallized basaltic rock and altered basaltic glass, and the rapid transition from silica to calcite-rich veins.

Within the glassy margins, symmetric rims of yellowish brown to orange altered basaltic glass (palagonite) are developed along fractures and cracks. Within individual margins, the thicknesses of altered glass layers vary from 300 µm to hardly visible, suggesting several generations of cracks and/or different alteration rates (Fig. F16). The thickness of altered glass may also vary along individual cracks. Generally, the altered glass rims show weak parallel zoning; however, at the alteration front, dendritic features are commonly observed extending into fresh glass, and these are believed to be related to microbial degradation of the glass (Fig. F17). The outer parts of the alteration rims consist of crystalline smectite, whereas the inner parts are amorphous and darker in color (Fig. F18). Within veins, the outer surface of the altered glass is often lined with thin layers (2–10 µm) of Fe oxyhydroxide and/or silica.

In the highly and moderately altered sections, as much as 80% of olivine phenocrysts are replaced by Fe oxyhydroxide and clay; rarely, as much as 20% of plagioclase is altered cloudy white. In slightly altered pieces, olivine is partially to completely altered to Fe oxyhydroxide and clay only within the oxidation halos of fractures, whereas plagioclase

F10. Vesicles filled with smectite and smectite and calcite, p. 23.

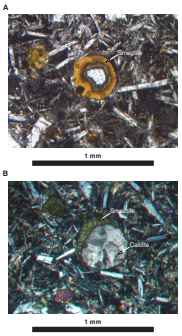

F11. Calcite-filled veins perpendicular to chilled margin in basalt, p. 24.

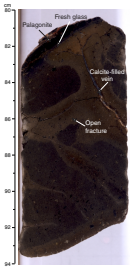

F12. Partially palagonitized pillow margin with calcite veins and micritic calcite, p. 25.

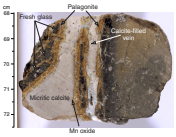

F13. Radial sparry calcite growth on micritic calcite in a vein, p. 26.

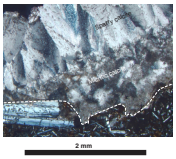

F14. Mn oxide blebs around recrystallized calcite crystals in a calcite vein, p. 27.

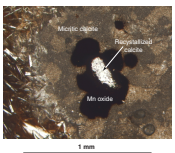

remains mostly fresh throughout, even when crosscut by calcite veins (Fig. F19). The groundmass is variably altered through replacement of olivine, clinopyroxene, and mesostasis to smectite and Fe oxyhydroxide, and visible as intense or patchy change to grayish green. Groundmass plagioclase usually remains fresh. Patchy groundmass alteration forms a crude network along which alteration appears to have progressed and split the rock into smaller alteration domains. In summary, alteration in Hole 1155B is mainly controlled by high fracture densities (see "Structural Geology," p. 7). Micritic limestone associated with the basalt is a likely source for the calcite vein fillings.

MICROBIOLOGY

At Site 1155 five rock samples (Samples 187-1155A-2R-1 [Piece 1A, 0–3 cm], 187-1155B-2R-1 [Piece 6A, 60–63 cm], 187-1155B-3R-1 [Piece 6A, 30–32 cm], 187-1155B-5R-1 [Piece 14A, 120–123 cm], and 187-1155B-8R-1 [Piece 16A, 109–114 cm]) were collected to characterize the microbial community inhabiting this environment (Table T2). All samples are pillow basalt fragments, including both the partly altered glassy margin and the more crystalline interior. To sterilize them, the outer surfaces of the rock samples were quickly flamed with an acetylene torch. Enrichment cultures and samples for high-pressure enrichment, DNA analysis, and electron microscope studies were prepared (see "Igneous Rocks," p. 7, in "Microbiology" in the "Explanatory Notes" chapter).

To evaluate the extent and type of contamination caused by drilling fluid, fluorescent microsphere tests were carried out for three rock cores and surface seawater was collected for DNA characterization (see "Tracer Test," p. 9, in "Microbiology" in the "Explanatory Notes" chapter and Table T2). One or two pieces from each core were rinsed in nanopure water, the collected water was filtered, and the filters were examined for the presence of microspheres under a fluorescence microscope. Thin sections were used to examine the extent of contamination inside the samples. Microspheres were detected on all three filters but were not seen in any of the thin sections.

STRUCTURAL GEOLOGY

Hole 1155A

The principal deformation structures developed in basalts from Site 1155 are fractures and veins. In basalts from Hole 1155A, the total number of fractures + veins recorded per meter of core (*N*/m) averages 6.5/m (ranging from 1.8 to 10.8/m), which is similar to Sites 1152 and 1154 (6.45 and 6.85/m, respectively). Veins, filled by calcite, clay, or silica (see "Alteration," p. 5) are developed only in Cores 187-1155A-5R through 7R. The average number of veins per meter of recovered core (vein density) is 2.2/m (ranging from 0 to 4.3/m).

Hole 1155B

In basalts from Hole 1155B, both fractures and veins are common throughout. The fracture + vein density averages 19.4/m (ranging from

F15. Aragonite and Mn oxide lining a calcite vein, p. 28.

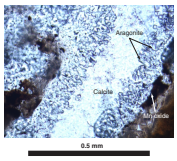

F16. Basaltic glass altered to palagonite, p. 29.

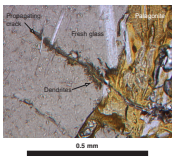

F17. Interface between fresh and altered basaltic glass, p. 30.

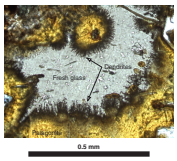

F18. Calcite vein, palagonite, and dentritic alteration front permeating fresh basaltic glass, p. 31.

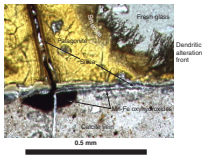

F19. Plagioclase crosscut by calcite vein unaffected by alteration, p. 32.

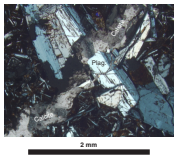

T2. Rock samples for cultures, DNA analysis, SEM/TEM, and contamination studies, p. 40.

6.7 to 40.2/m), and the vein density averages 12.4/m (ranging from 0 to 30.3/m). Vein widths are mostly <2 mm.

SITE GEOPHYSICS

Site 1155 was located based on 1997 SCS site survey data and confirmed by a short 3.5-kHz PDR and SCS presite survey from the *JOIDES Resolution* (JR). Onboard instrumentation used included a precision echo sounder, gyrocompass, seismic system, and GPS receivers.

Seismic Reflection Profiling

Site selection for Site 1155 was based on a north-south SCS survey conducted during the *R/V Melville* cruise Sojourner 5 in 1997. A 1.2-hr SCS and 3.5-kHz PDR survey was conducted on the approach to Site 1155 (JR SCS line S3; Fig. **F20**) to ensure the correct site location. The ship's average speed was 5.0 kt during the survey. The water gun was triggered at a shot interval of 12 s, equivalent to ~31 m at 5.0 kt. Data acquisition and processing parameters were described in **"Underway Geophysics,"** p. 10, in the "Explanatory Notes" chapter. Survey line S3 was conducted in an east-west direction, perpendicularly across the previous survey line. The final position of Site 1155 is almost identical to the prospectus site AAD-35a and is located at the crossover point of these two survey lines. We marked the position of Hole 1155A near seismic shotpoint 144 of line S3, where the water depth is 4986.4 m (see Fig. **F21**) and where the sediment cover is apparently thicker than elsewhere. The sediment cover (Fig. **F21**) extends from 6.70 s to at least 6.85 s in two-way traveltime, equivalent to 150–200 m of sediment. Hole 1155A was drilled through 177 m of sediment before basement was reached, confirming the above estimate. Hole 1155B was shifted ~200 m west of Hole 1155A, near shotpoint 150.

F20. Track chart of the JR SCS survey line S3, p. 33.

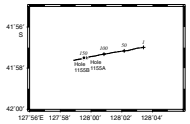

F21. SCS profile of line S3 from shots 1 to 175, p. 34.

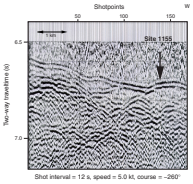

SEDIMENTS

The first core recovered from Hole 1155A was a wash barrel that sampled the interval from the seafloor to 177.3 mbsf. Although all the sediment recovered is clay, we have subdivided the recovered material into four informal zones based on variations in color and composition (Fig. **F22**). These zones imply no stratigraphy, except that, based on the lack of evidence of severe drilling disturbance throughout most of the section, the sediment types have not been displaced vertically relative to each other.

Zone A (0.0–0.57 m in Section 187-1155A-1W-1) is a siliceous pelagic clay. The upper 50 cm of this interval is very soupy and contains abundant, coarse, sand-sized clay pellets. The lower 7 cm of this interval is significantly less disturbed by drilling and has a slightly lighter color. At 57 cm there is a sharp contact with Zone B. The contact is marked by a break in the core, suggesting an interval of no recovery rather than a stratigraphic contact. Zone B is a homogeneous dark grayish brown siliceous clay, which extends to 70 cm in Section 187-1155A-1W-2. The bottom of Zone B is marked by a planar but diffuse (>1 mm) contact with medium light brown calcareous clay. The calcareous clay marks the top of Zone C (0.70–0.90 cm in Section 187-1155A-1W-2). Zone C was defined because, below a 5-cm-thick calcareous interval, another

F22. Sediment zone determination, p. 35.

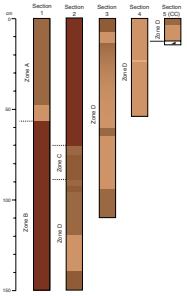

10-cm-thick siliceous clay, devoid of calcite, is present. This is distinctive in that, in all the sediments we have recovered so far, the division between siliceous clay and calcareous clay is a compositionally well-defined break. Zone D (Section 187-1155A-1W-2, 90 cm, to the bottom of the core) is all calcareous clay but exhibits distinct to subtle color changes. Within this interval are several 3- to 25-cm-thick layers of medium dark brown clay intercalated with intervals of light brown clay. Most of these intervals have planar but diffuse (>1–2 mm) contacts, although in Section 187-1155A-1W-4, a 1-cm-thick dark layer is dipping about 20° across the core face and also has an 0.5-cm offset apparent in the cut face of the core. At 23.5 cm in Section 187-1155A-1W-4 is a disseminated, very fine grained black silt marking the top of a 0.5-cm-thick very light yellow-brown layer. This layer has diffuse upper and lower contacts (>1 mm) with the light brown calcareous clay above and below.

A smear slide from Zone A contains abundant honeycomb-textured fragments of radiolarians, as well as colorless translucent spines. Rare cigar-shaped microfossils with visible septa are also present. All clay pellets from Zone A completely disaggregate in water, suggesting that they formed during drilling. Zone B and the siliceous sediment from Zone C contain 1%–2% subrounded brown volcanic glass fragments (3 to 4 µm across) and much more rare colorless crystal shards and siliceous microfossil fragments. The calcareous clay of Zones C and D contains abundant microfossils and <1% brown volcanic glass and crystal shards. Abundant calcareous microfossils predominate in the thin light yellow-brown interval in Section 4, to the exclusion of most other components in other sediment intervals from this core. In a smear slide, the thin disseminated black silt at the top of this layer appears to consist of 25- to 50-µm-sized fragments of dark volcanic glass. A 2-cm fragment of altered volcanic glass was embedded in the sediment at the bottom of the core.

Hole 1155B recovered 28 cm of dark brown homogeneous siliceous clay, similar in appearance to the material in Zone B of Hole 1155A. No calcareous clay was recovered from this hole.

GEOCHEMISTRY

Introduction

Site 1155 basalts were recovered from two holes that sampled ~25-Ma crust formed within Segment B5 of the Australian Antarctic Discordance. Seven whole-rock powders were analyzed for major and trace elements by X-ray fluorescence (XRF) and inductively coupled plasma–atomic emission spectrometry (ICP-AES); two glasses and one plagioclase separate were analyzed by ICP-AES only. The results are shown in Table **T3**. There are few discrepancies between XRF and ICP-AES analyses, except that Na_2O content is generally higher and Ni content is generally lower by ICP-AES.

T3. Glass and whole-rock compositions, Site 1155, p. 41.

Hole 1155A

Samples from Hole 1155A are assigned to two lithologic units based on macroscopic and microscopic examination (see **"Igneous Petrology,"** p. 3). Unit 1 is a sparsely to moderately plagioclase ± olivine phyric basalt pillow lava flow. Unit 2 consists of aphyric basalt pebble and

cobble fragments interpreted as unconsolidated rubble. Unit 1 is represented by a single whole-rock analysis, as there was insufficient glass for ICP-AES analysis. From Unit 2, one whole-rock and one glass sample were analyzed (Table **T3**). The Hole 1155A Unit 2 glass is higher in MgO (7.8 wt%) than both Unit 2 and Unit 1 whole rocks (Fig. **F23**). The Unit 1 whole rock (6.9–7.1 wt% MgO) is slightly more evolved than that of Unit 2 (7.2–7.3 wt% MgO). Higher TiO_2, Zr, and Ni and lower Cr and Sr in Unit 1 suggest that Units 1 and 2 are not related by simple crystal fractionation (Fig. **F24**). The Unit 2 glass is also higher in Fe_2O_3, Na_2O, and Ba and lower in Al_2O_3, CaO, Sr, and Ni than whole rocks from both units, indicating that they are also not related by simple low-pressure crystal fractionation. Similarities in TiO_2, Zr, Y, and Cr contents suggest that Unit 2 glass is more like Unit 1 whole rocks than its spatially related Unit 2 whole rocks. Given that the glass sample from Unit 2 was a small pebble, it is possible that this piece fell into the hole from Unit 1 above. This is consistent with our observation, based on larger pieces (e.g., Section 187-1155A-5R-1 [Piece 3]) that such fall-in has occurred in this hole (see **"Unit 2,"** p. 4, in "Igneous Petrology").

Hole 1155B

Hole 1155B samples are interpreted as derived from a single, intact pillow lava sequence of moderately plagioclase ± olivine phyric basalts. One glass and a plagioclase separate from that glass were analyzed by ICP-AES. Five whole rocks were analyzed by ICP-AES and XRF. The glass is primitive in composition and is higher in MgO (9.3 wt%) than associated whole rocks (7.9–8.5 wt% MgO). The whole rocks form a coherent group that shows evidence of simple crystal fractionation, but they are not a product of differentiation from the more primitive Hole 1155B glass composition. The glass is higher in Fe_2O_3 and Na_2O and lower in CaO, Al_2O_3, and Ni than Hole 1155B whole rocks, consistent with the observed phenocryst assemblage (i.e., plagioclase and olivine accumulation). The glass is also slightly higher in Zr, Y, and TiO_2. As in samples from Hole 1155A and the majority of holes sampled, glasses and whole rocks recovered within a single hole usually are not easily related by simple crystal fractionation. In most cases, it appears that MgO has been selectively removed from the whole rock samples by low-temperature alteration. Other processes including mineral accumulation and nonequilibrium fractionation may also have affected the whole-rock compositions.

The plagioclase separate and Sample 187-1155B-2R-1, 125–129 cm, a highly unusual low-MgO basaltic sample, are not shown in Figures **F23** and **F24** because they lie out of the typical basalt range and therefore outside the figures. This basalt differs from other whole rocks by its extremely low MgO content and high Al_2O_3, CaO, Fe_2O_3, Sr, and, to some extent, Na_2O. There is no evidence of extreme plagioclase accumulation or of excessive loss on ignition (LOI) values, which typically indicate intense alteration. However, thin-section examination reveals a groundmass extensively replaced by clay and Fe oxyhydroxide; therefore, this composition most likely, but not obviously, represents an extreme alteration effect, despite the low LOI (see **"Alteration,"** p. 5). There is little evidence to suggest this composition is a product of magma evolution. Surprisingly, its Ba is indistinguishable from "unaltered" samples.

F23. Major element compositions vs. MgO of basalts, Holes 1155A and 1155B, p. 36.

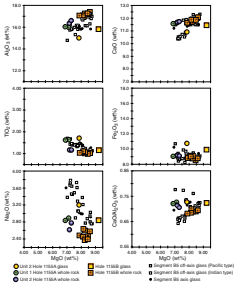

F24. Trace element compositions vs. MgO for basalts, Holes 1155A and 1155B, p. 37.

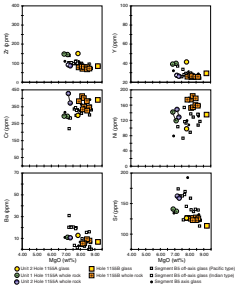

Temporal Variations

Site 1155 is the first site of Leg 187 within Segment B5. At present, Segment B5 lies toward the eastern side of the depth anomaly; it displays much of the range of axial morphology mapped in this area, and its western transform boundary is the current position of the Indian-Pacific isotopic boundary. For some elements, Site 1155 basalts show the same major and trace element variations seen on or near the B5 spreading axis (Figs. **F23, F24**). However, Site 1155 glasses have distinctly higher TiO_2, Fe_2O_3, Zr, and Y and lower Al_2O_3 for a given MgO content. The only apparent evidence of a significantly different melt regime at 25 Ma is high Fe_2O_3, which, in the absence of other compositional evidence, may imply a deeper mean melting depth (Langmuir et al., 1993). More likely, the compositional variations between Site 1155 lavas and present Segment B5 axis lavas are caused by variations in mantle composition; cooler or warmer mantle melting conditions are less likely because other melting indicators, such as CaO/Al_2O_3 and Na_2O, are the same as for younger dredge samples.

Mantle Domain

The Zr/Ba systematics of Site 1155 (Fig. **F25A**) suggest that both Indian- and Transitional-Pacific–type mantle were present beneath this site when it was at the spreading axis. The Hole 1155A Unit 2 glass and the Hole 1155A Unit 1 whole rock have relatively high Zr/Ba and low Na_2O/TiO_2 values (Fig. **F25B**), which indicate a Transitional-Pacific–type source (see **"Barium and Zirconium,"** p. 13, in the "Leg Summary" chapter). On the other hand, Hole 1155B glass and whole rocks, as well as Hole 1155A Unit 2 whole rock, lie well within the range of Zr/Ba vs. Ba variations for Indian-type mantle; these samples lie along a low-Ba trend similar to that defined by Segment B5 axial samples that span the Indian- to Pacific-type ranges.

To test whether plagioclase accumulation could account for the coherent grouping of glasses and whole rocks along curved trends on the Zr/Ba vs. Ba diagram, a plagioclase separate was handpicked from Hole 1155B glass and analyzed by ICP-AES. The position of the plagioclase in Figure **F25A** clearly demonstrates that plagioclase accumulation cannot drive the negative Zr/Ba vs. Ba variations. In fact, this plagioclase is low in Ba content, and varying its abundance in small proportions would have little effect on the observed trends. We also investigated whether simple crystal fractionation could, for instance, move compositions from Hole 1155B glass to Hole 1155A glass on the Zr/Ba vs. Ba diagram. An arrow in Figure **F25A** shows ~50% fractional crystallization at low pressure. The trajectory of the trend is clearly toward Hole 1155A glass. However, to achieve this, MgO would be required to decrease to ~5.1 wt%, much lower than any Hole 1155A composition. Therefore, observed variations in Zr/Ba vs. Ba are not caused by simple low-pressure crystal fractionation or plagioclase accumulation.

Neither simple melting nor simple mixing variations can fully account for the difference between Hole 1155A and Hole 1155B compositions. Simple batch melting within either a Pacific- or Indian-type source moves values up and down along negative curves. At least two "enriched" end-members, an Indian type and one similar to propagating rift tip (PRT) lavas, and one or two "depleted" end-members are required to produce the curves. Varying the proportions of Pacific- and Indian-type source melts moves compositions between the two trends

F25. Variations of Zr/Ba vs. Ba and Na_2O/TiO_2 vs. MgO, Hole 1155A and Hole 1155B, p. 38.

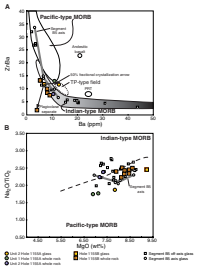

(e.g., varying the Ba composition of the source). For example, in the transitional region between the Pacific- and Indian-type fields (i.e., Zr/Ba = 10–15 and Ba = 8–15 ppm), as Ba increases, we expect mixing to shift toward a curve that includes the Pacific-type field and the Zone A PRT lavas; therefore, the rock would be of a Pacific-type affinity or, as we have defined, Transitional-Pacific type. The Indian-type curved field is offset toward lower Ba content. The way the Indian- and Pacific-type fields overlap one another in Zr/Ba at distinct Ba concentrations demonstrates that subtle shifts in the Ba concentration of mantle sources affect the position of mixing and melting curves on this diagram and therefore our designation of the mantle domain from which the basalts derived.

REFERENCE

Langmuir, C.H., Klein, E., and Plank, T., 1993. Petrological systematics of mid-ocean ridge basalts: constraints on melt generation beneath ocean ridges. *In* Morgan, J., Blackman, D., Sinton, J. (Eds.), *Mantle Flow and Melt Generation at Mid-Ocean Ridges*. Geophys. Monogr., Am. Geophys. Union, 71:183–277.

Figure F1. Photograph of interval 187-1155B-8R-3, 68–72 cm, showing micritic limestone infilling a fracture and an interpillow space.

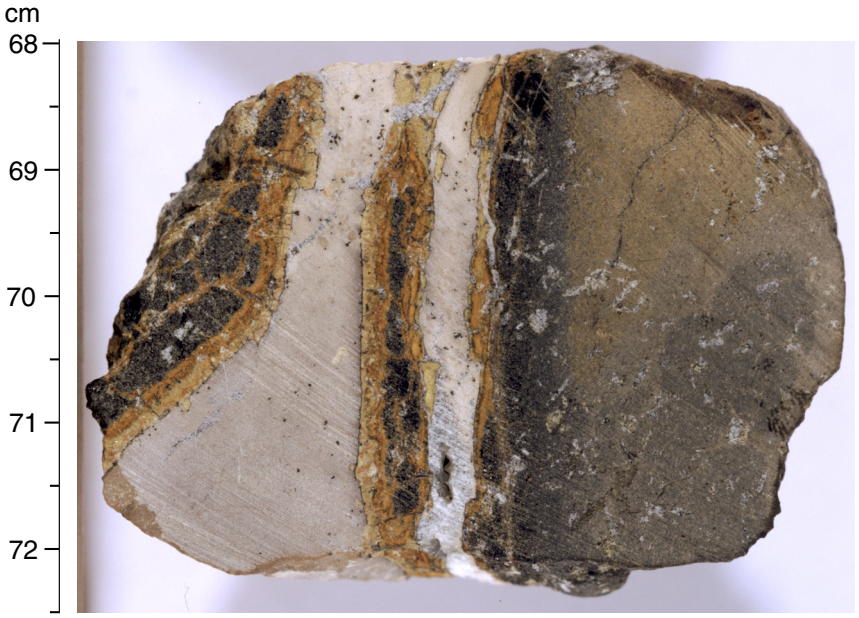

Figure F2. Photograph of interval 187-1155B-9R-1, 26–34 cm, showing a sparry calcite vein and micritic limestone infilling a fracture running perpendicular to the chilled margin (darker colored band in the top centimeter of the piece).

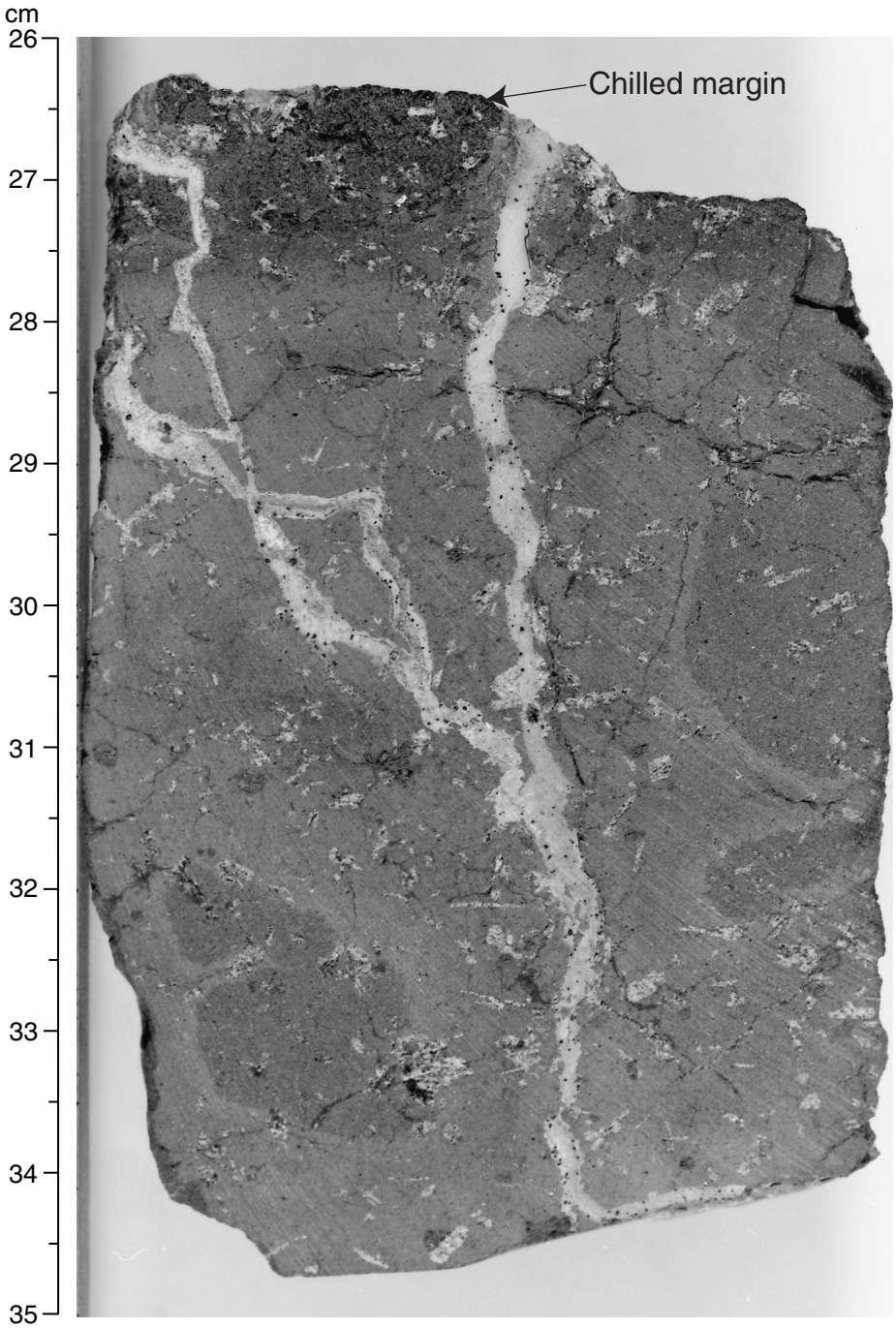

Figure F3. Photomicrograph, with crossed polars, of Sample 187-1155A-2R-1, 29–32 cm (see **"Site 1155 Thin Sections,"** p. 29), showing a vesicle lined with smectite and filled with calcite. Notice the intersertal groundmass texture.

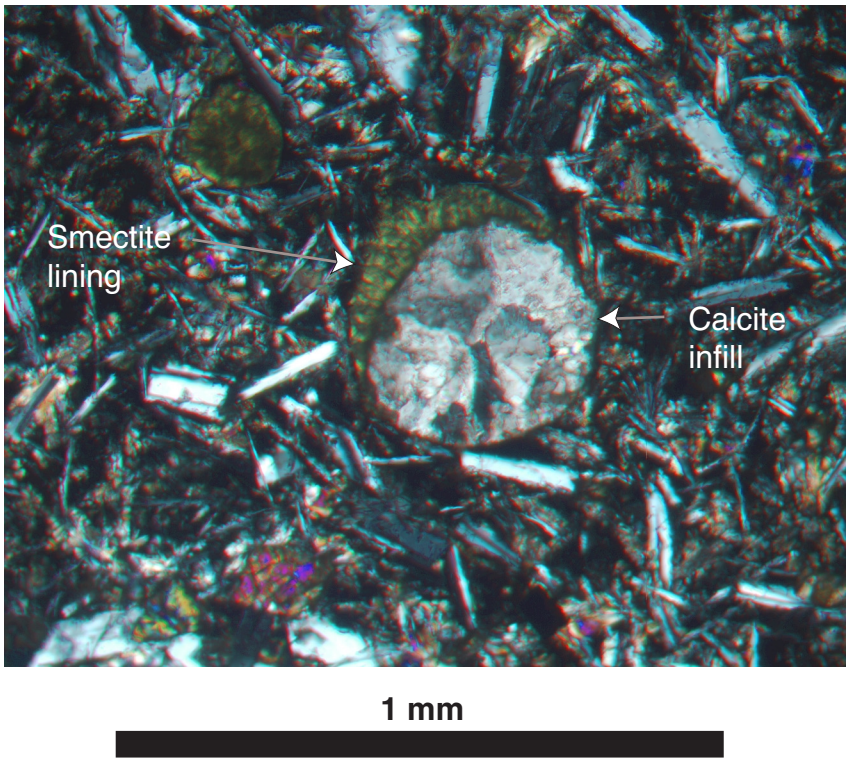

Figure F4. Photomicrograph, with crossed polars, of Sample 187-1155A-7R-1, 16–19 cm (see "Site 1155 Thin Sections," p. 30), showing a sieve-textured plagioclase phenocryst rounded by resorption. Groundmass shows intersertal texture typical of this unit.

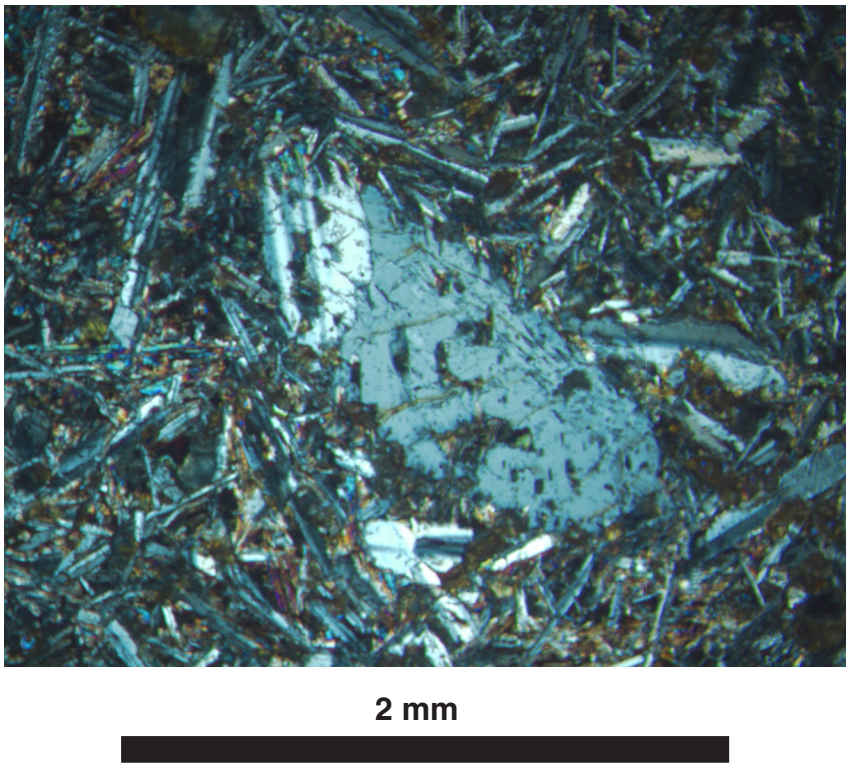

Figure F5. Photomicrograph, with crossed polars, of Sample 187-1155B-9R-1, 119–122 cm (see "Site 1155 Thin Sections," p. 39), showing a sieve texture in the core of a plagioclase phenocryst.

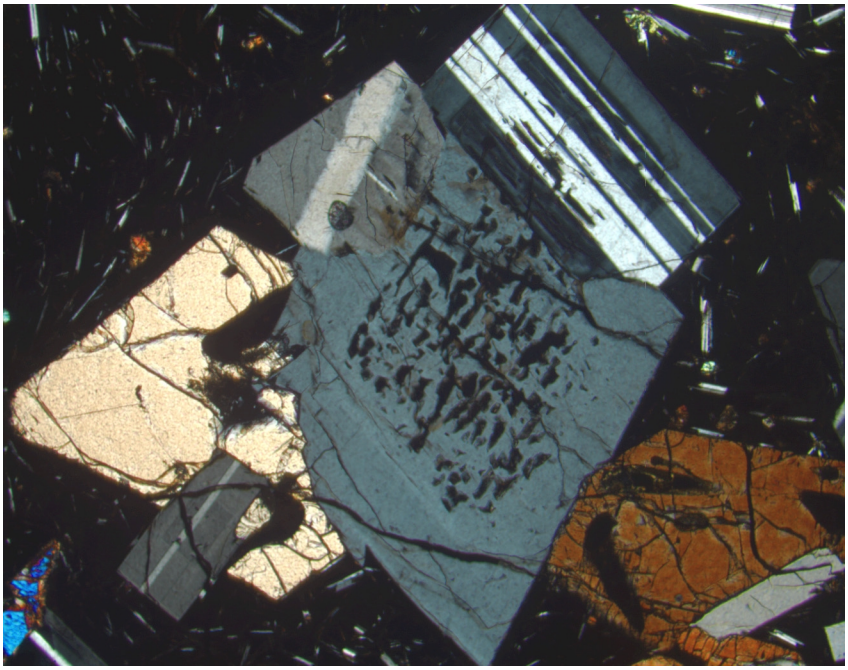

Figure F6. Photomicrograph in plane-polarized light of Sample 187-1155B-2R-1, 125–129 cm (see "Site 1155 Thin Sections," p. 32), showing a Cr spinel included in a plagioclase phenocryst.

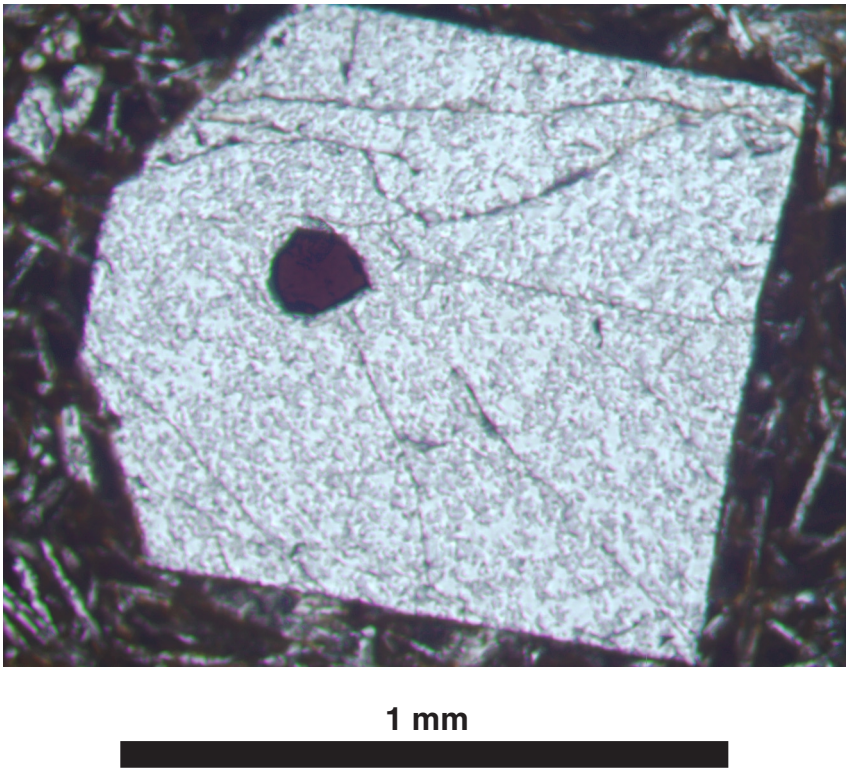

Figure F7. Photomicrograph in plane-polarized light of Sample 187-1155B-7R-1, 62–65 cm (see **"Site 1155 Thin Sections,"** p. 37), showing a Cr spinel included near the edge of a plagioclase phenocryst. Notice the intersertal groundmass texture (top of the image) with skeletal plagioclase microlites.

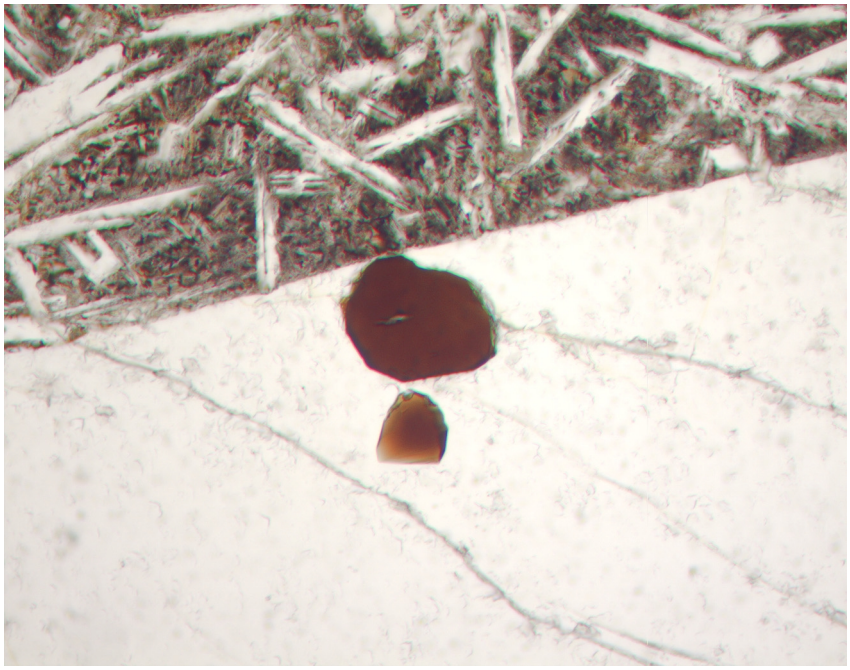

Figure F8. Photomicrograph in plane-polarized light of Sample 187-1155B-2R-1, 68–71 cm (see **"Site 1155 Thin Sections,"** p. 31), showing a plagioclase phenocryst abutting a calcite vein. Notice the weak flow alignment defined by the microphenocrysts (left half of the image).

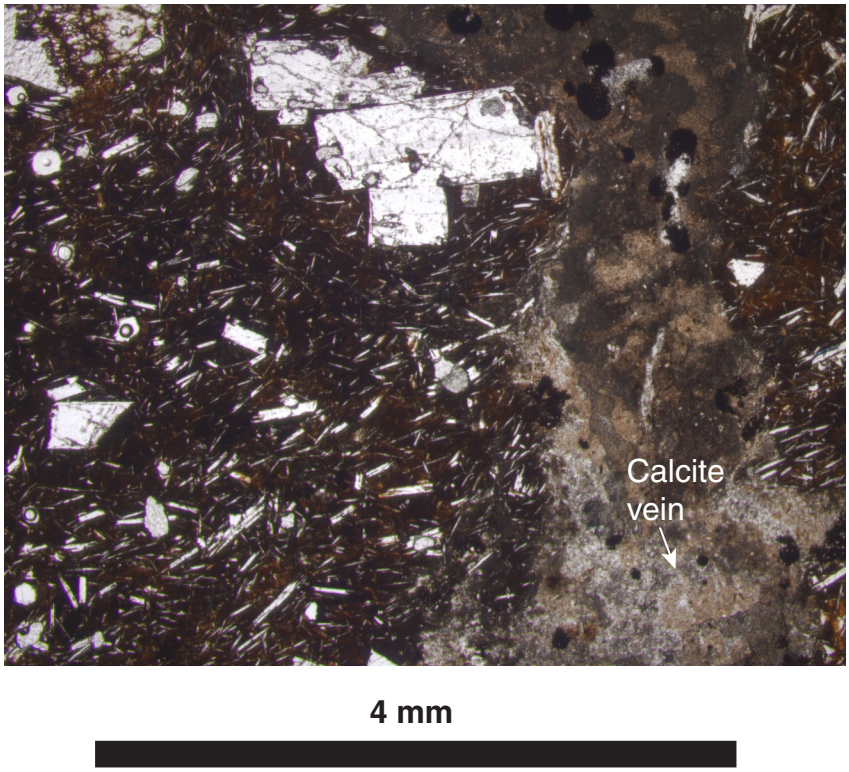

Figure F9. Photomicrograph in plane-polarized light of Sample 187-1155B-6R-3, 135–138 cm (see "Site 1155 Thin Sections," p. 36), showing a quench zone grading from fresh glass to spherulitic glass to coalesced spherulites. Notice the flow-aligned acicular plagioclase on which some spherulites have nucleated. The tan–brown transition at the first appearance of spherulites is due to the palagonitization of the glass.

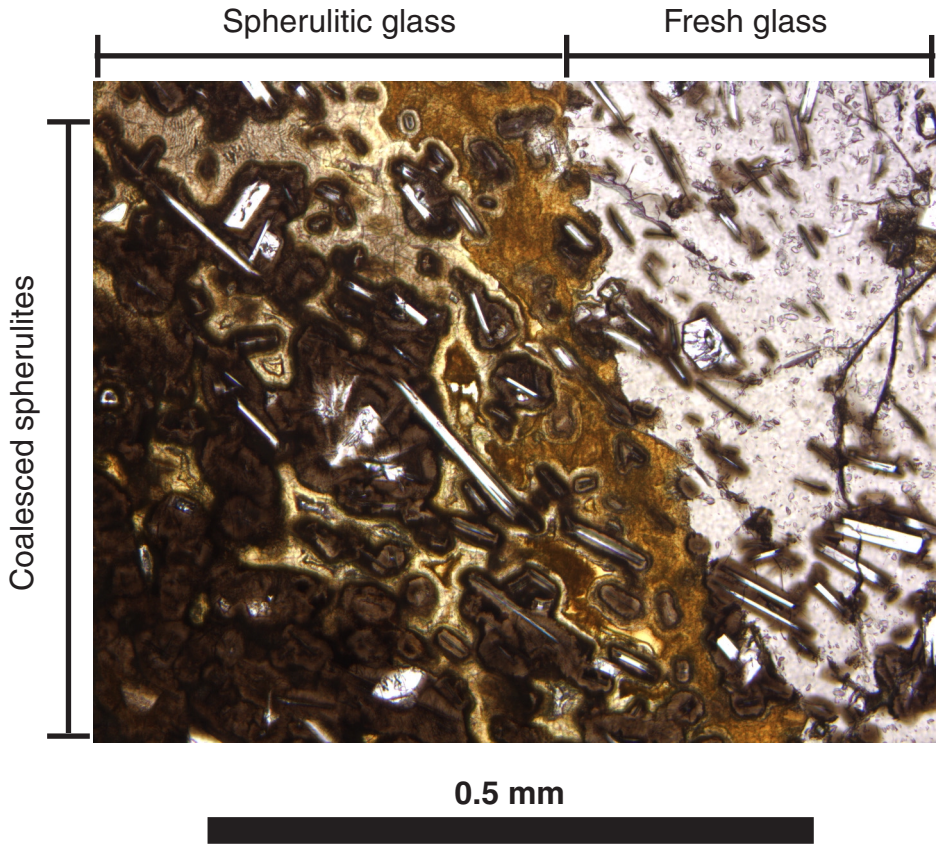

Figure F10. Photomicrographs in plane-polarized light of Sample 187-1155A-2R-1, 29–32 cm (see "Site 1155 Thin Sections," p. 29), showing vesicles filled with (**A**) smectite and (**B**) smectite and calcite.

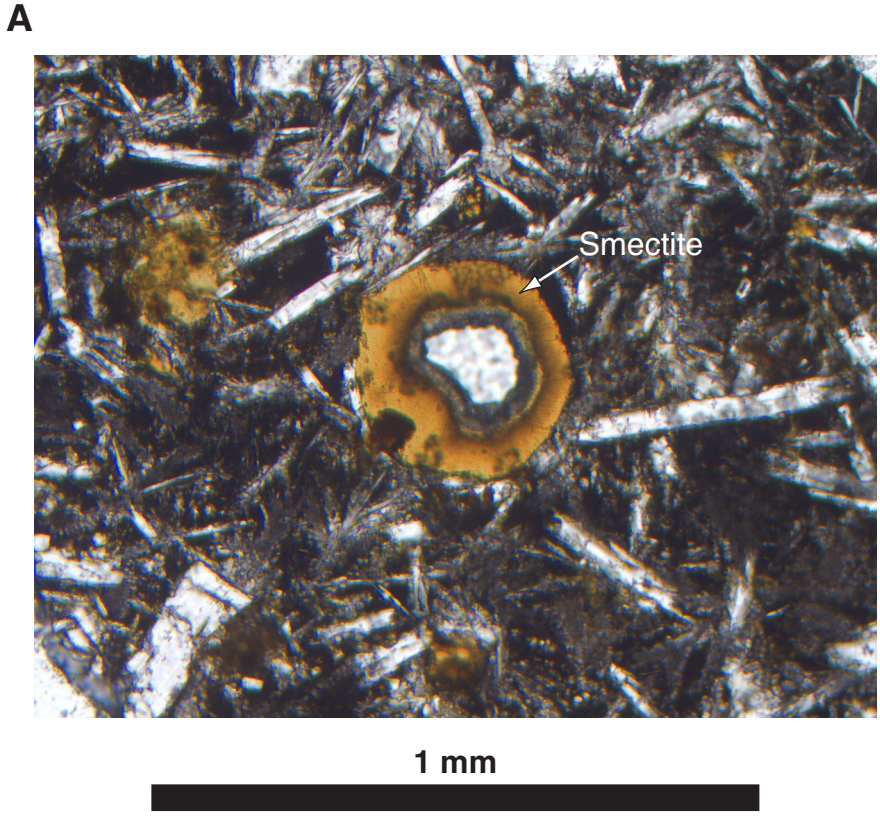

Figure F11. Photograph of interval 187-1155B-4R-2, 80–94 cm, showing calcite-filled veins forming an orthogonal set, with the largest fracture aligned perpendicular to the chilled margin. Fractures are surrounded by alteration halos. Note the branching of fractures near the glass margin.

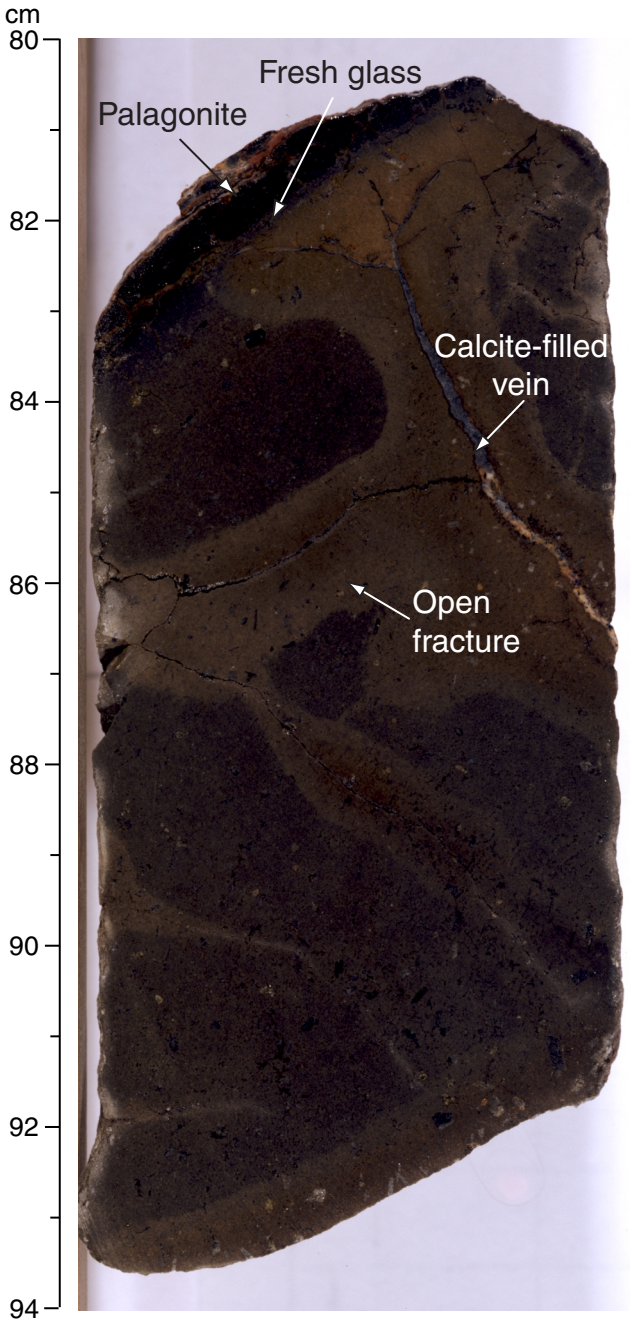

Figure F12. Photograph of interval 187-1155B-8R-3, 68–72.5 cm, showing a pillow margin with calcite veins running parallel to the glass margin and an associated wedge-shaped infill? of micritic calcite. Fresh glass is enclosed by palagonite. The boundary between the calcite vein/micritic limestone and altered glass is marked by a thin black layer of Mn oxide. Spotty Mn oxide is present within the calcite vein and the limestone.

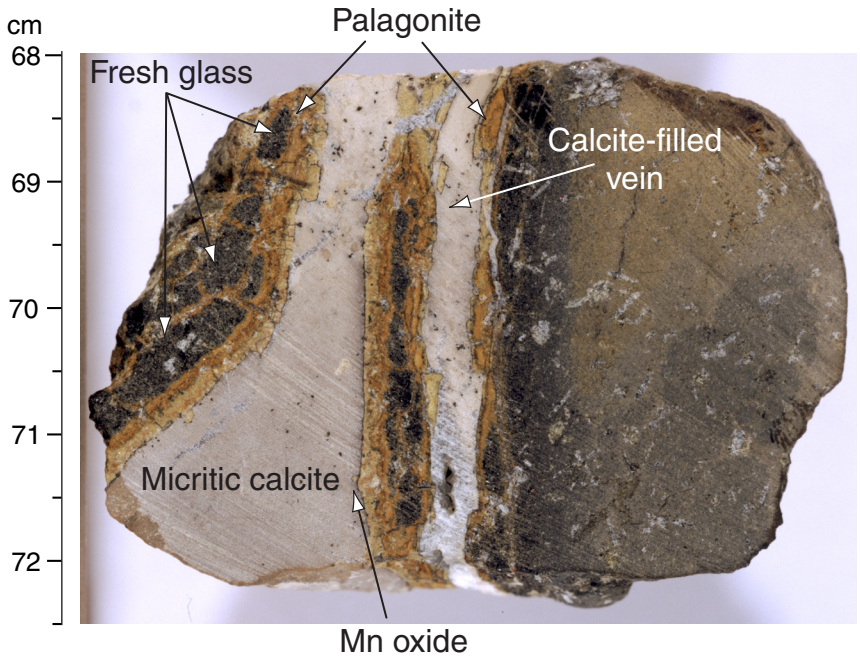

Figure F13. Photomicrograph, with crossed polars, of Sample 187-1155B-6R-2, 0–3 cm (see "Site 1155 Thin Sections," p. 35), showing sparry calcite growing perpendicular to the contact with micritic calcite. The inserted white dashed line follows the vein wall.

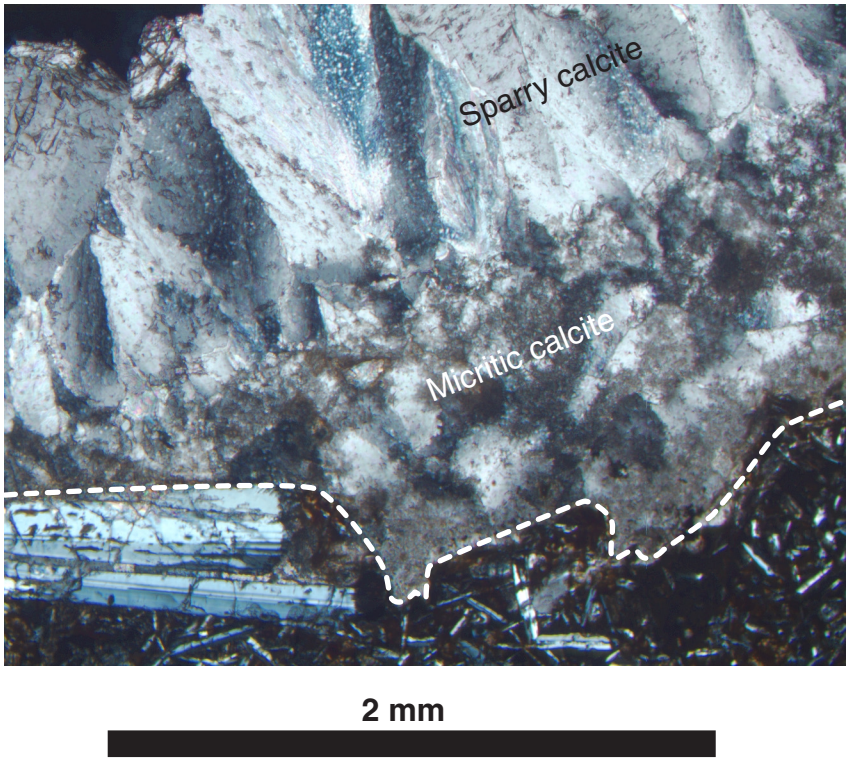

Figure F14. Photomicrograph in plane-polarized light of Sample 187-1155B-2R-1, 68–71 cm (see **"Site 1155 Thin Sections,"** p. 31), showing Mn oxide blebs growing around recrystallized calcite crystals within a calcite vein.

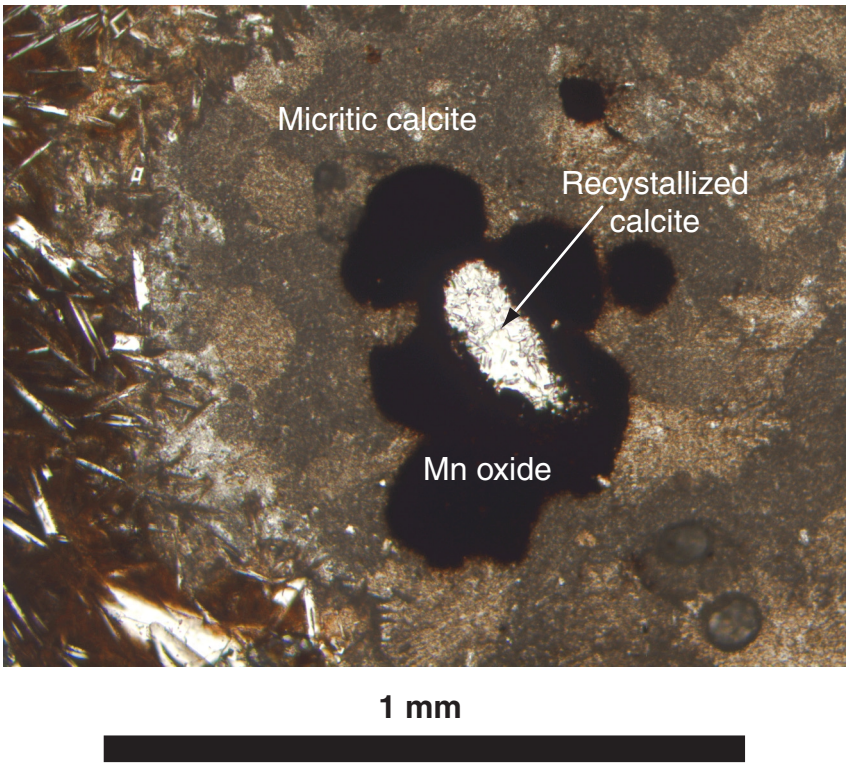

Figure F15. Photomicrograph in plane-polarized light of Sample 187-1155B-2R-1, 68–71 cm (see "Site 1155 Thin Sections," p. 31), showing aragonite crystals and Mn oxide lining a calcite vein.

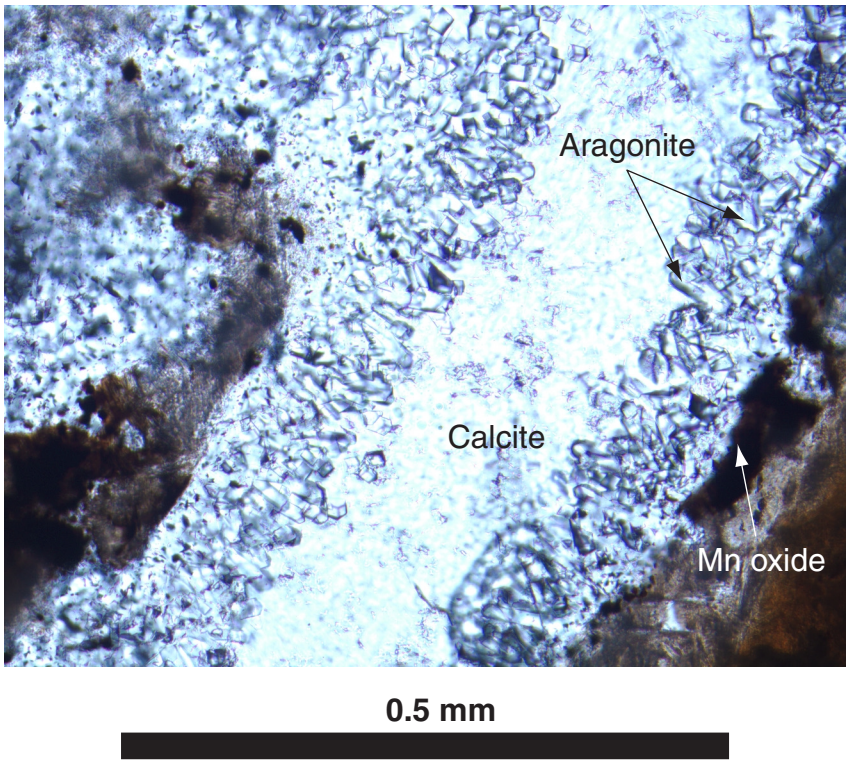

Figure F16. Photomicrograph in plane-polarized light of Sample 187-1155B-6R-3, 135–138 cm (see **"Site 1155 Thin Sections,"** p. 36), showing basaltic glass altered to yellowish brown-orange palagonite. Note the early stages of palagonitization surrounded by dendrites along the crack, aligned perpendicularly to the palagonitization front.

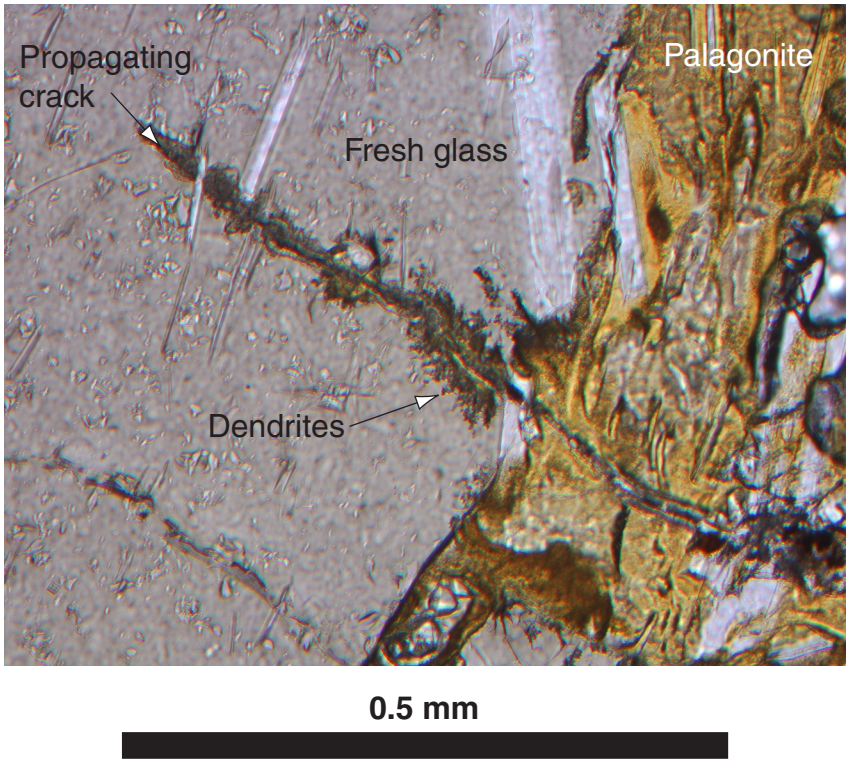

Figure F17. Photomicrograph in plane-polarized light of Sample 187-1155B-2R-1, 68–71 cm (see "Site 1155 Thin Sections," p. 31), displaying the interface between fresh and altered basaltic glass. Note the dendritic structures, believed to have formed by the biodegradation of glass.

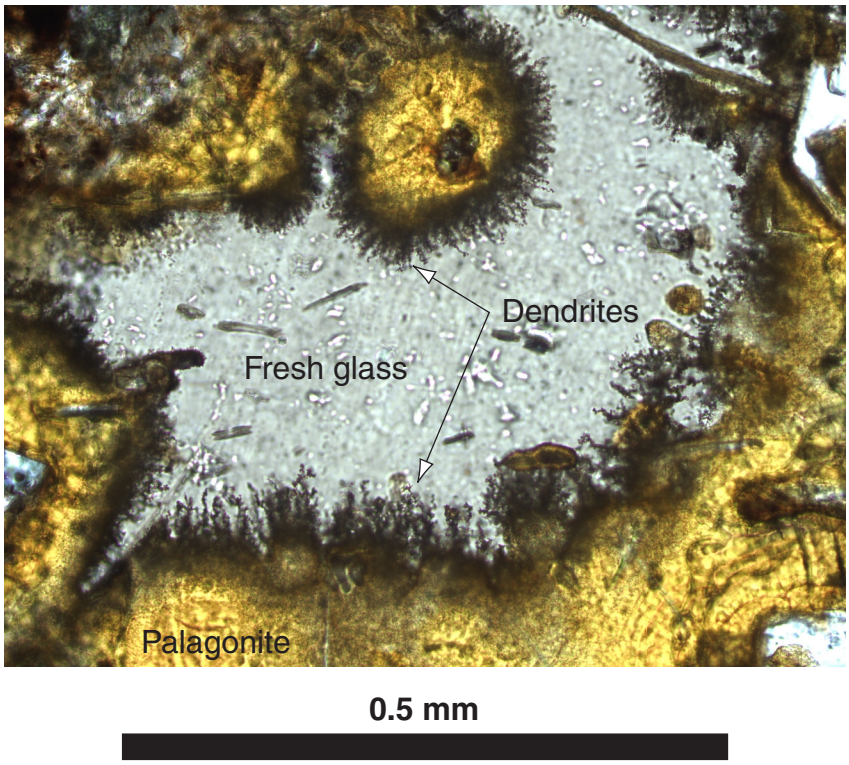

Figure F18. Photomicrograph in plane-polarized light of Sample 187-1155B-2R-1, 68–71 cm (see "Site 1155 Thin Sections," p. 31), showing the intersection of a calcite vein with palagonite. Silica and Fe oxyhydroxides line the edge of the calcite vein. Palagonite displays concentric zoning from cryptocrystalline to crystalline (smectite) toward the dendritic alteration front. The vertical fracture within the palagonite contains Fe oxyhydroxides and silica.

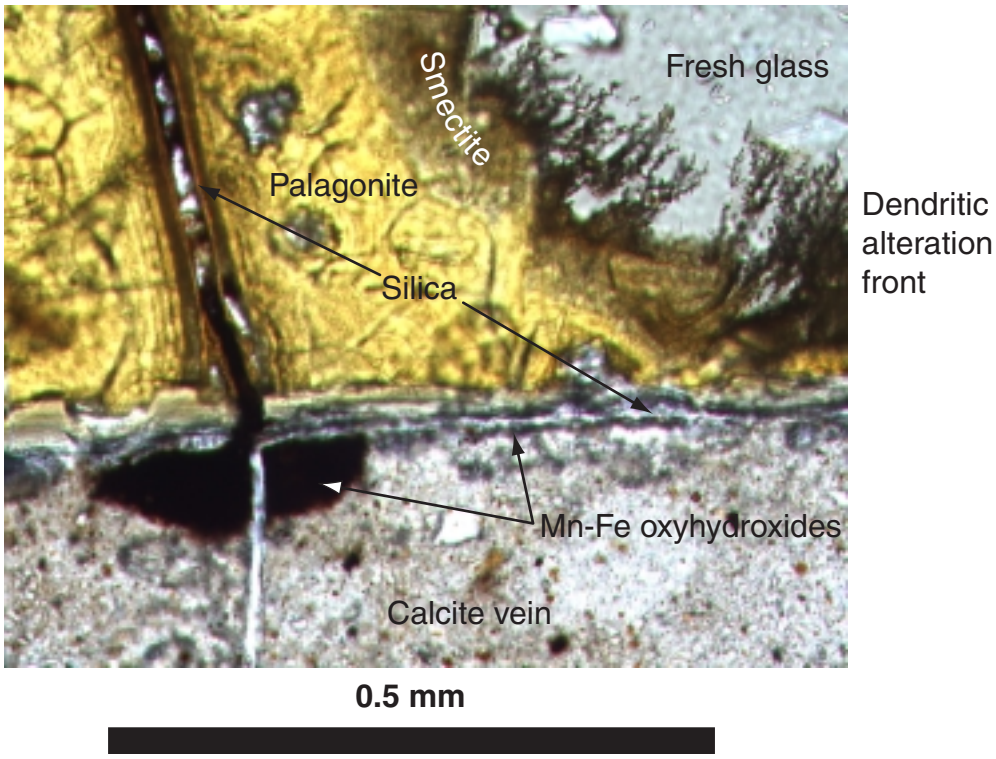

Figure F19. Photomicrograph of Sample 187-1155B-6R-2, 0–3 cm (see "Site 1155 Thin Sections," p. 35), showing that plagioclase (Plag.) crosscut by a calcite vein is mostly unaffected by alteration.

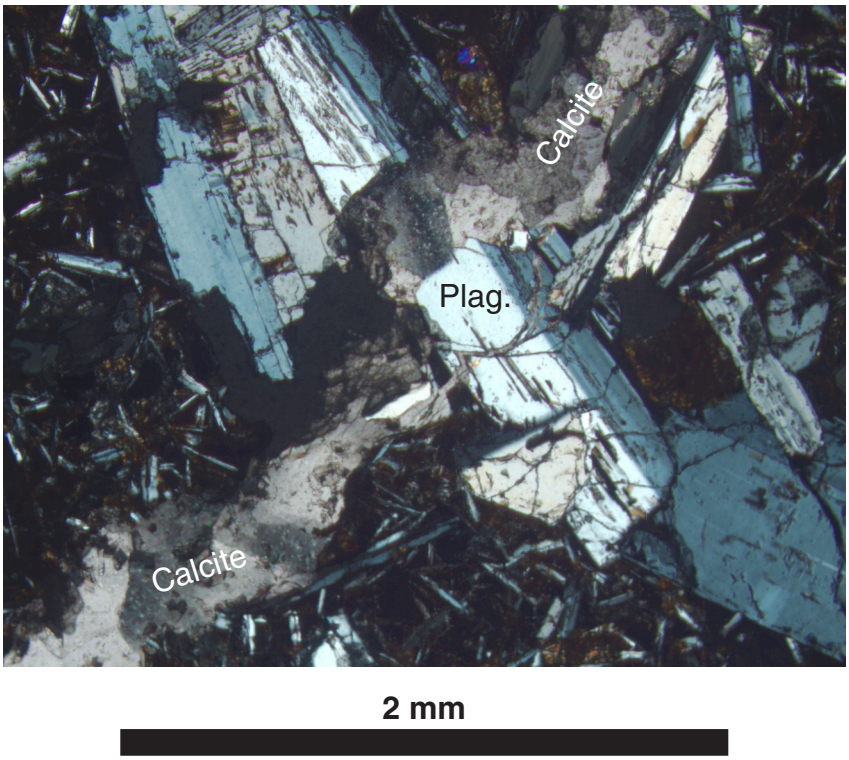

Figure F20. Track chart of the *JOIDES Resolution* single-channel seismic survey line S3. Crosses = 50-shot intervals. The positions of Holes 1155A and 1155B along the survey line are marked by solid circles. Survey line S3 was conducted from east to west.

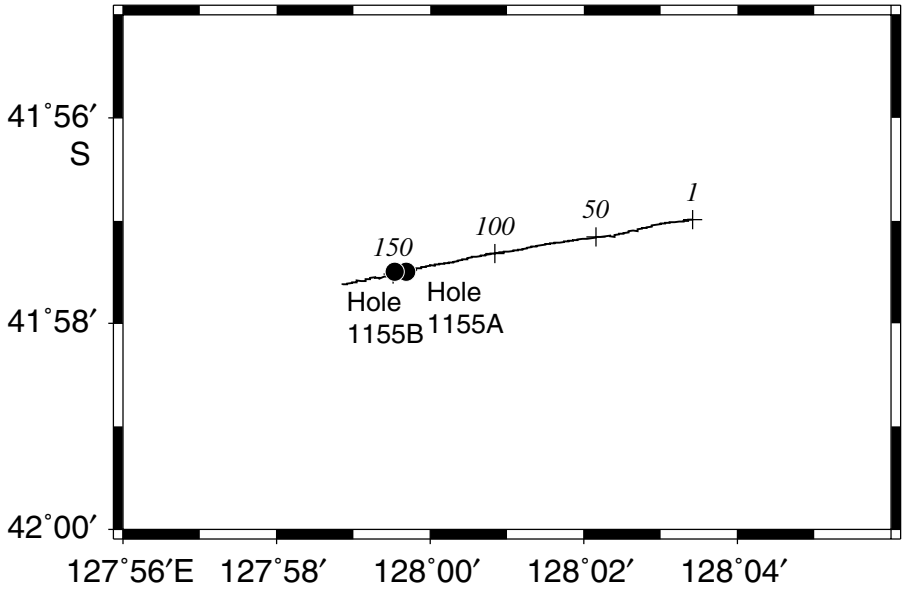

Figure F21. Single-channel seismic profile of line S3 from shots 1 to 175. A large arrow marks the position of Site 1155 near shotpoint 144. Apparently, the sediment cover here is thicker than elsewhere.

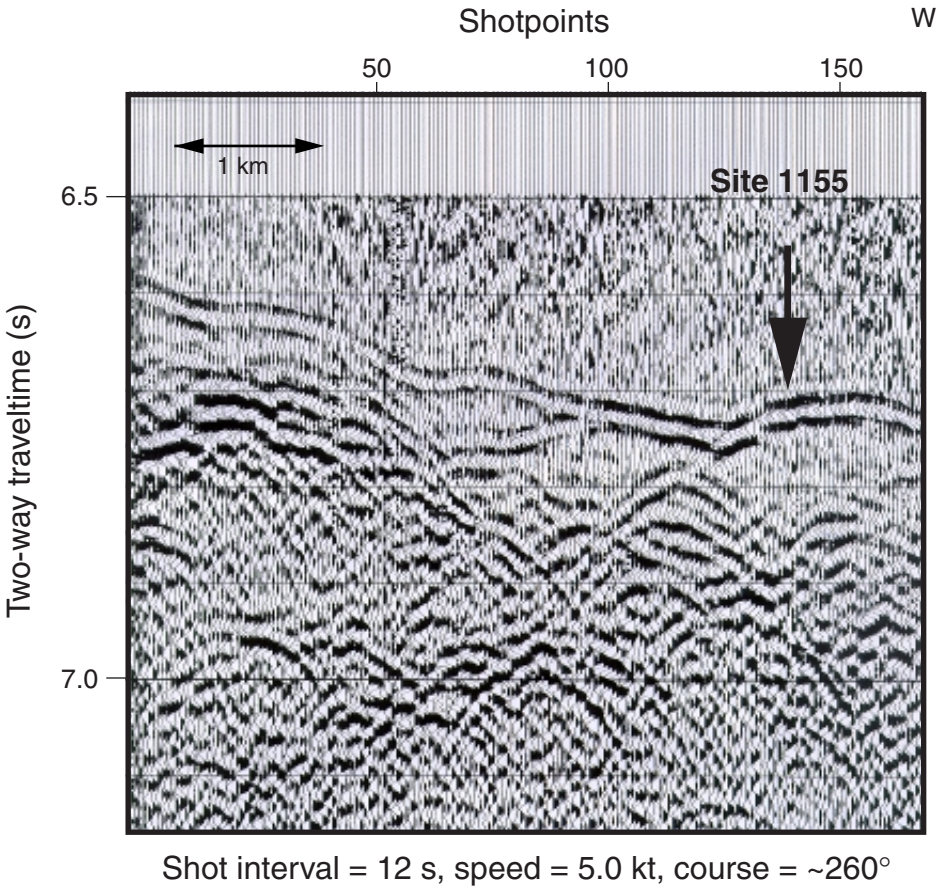

Figure F22. Sediment zone determination based on variations of color and composition for Core 187-1155A-1W. CC = core catcher.

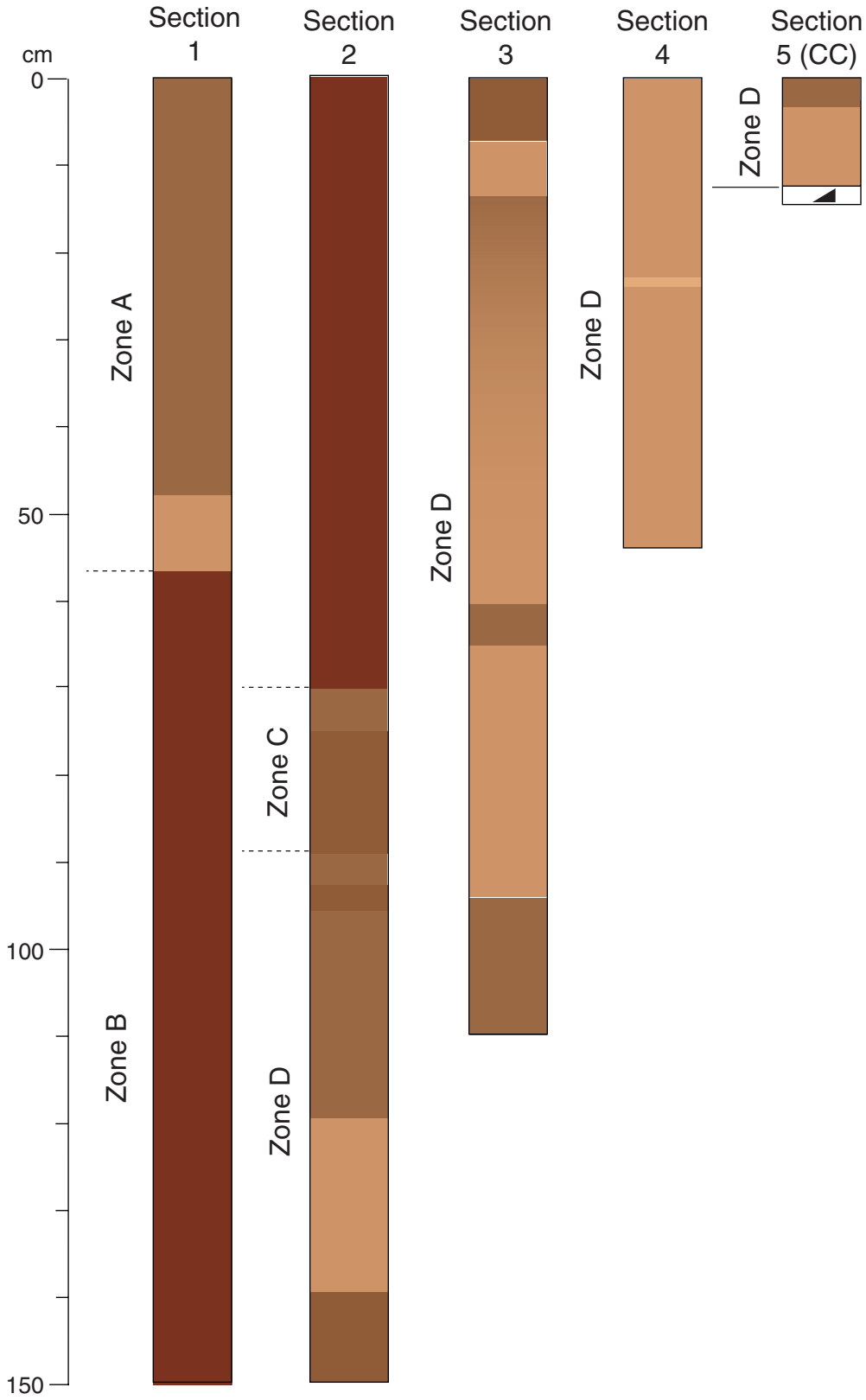

Figure F23. Major element compositions vs. MgO for basalts from Holes 1155A and 1155B compared with Southeast Indian Ridge glasses from Segment B5. X-ray fluorescence (XRF) and ICP-AES data for splits of a single whole-rock powder are shown on all plots. Two points represent each type of analysis for one sample. Only the average XRF or ICP-AES analyses reported in Table T3, p. 41, are plotted. The analytical bias between XRF and ICP-AES is most pronounced for Na_2O.

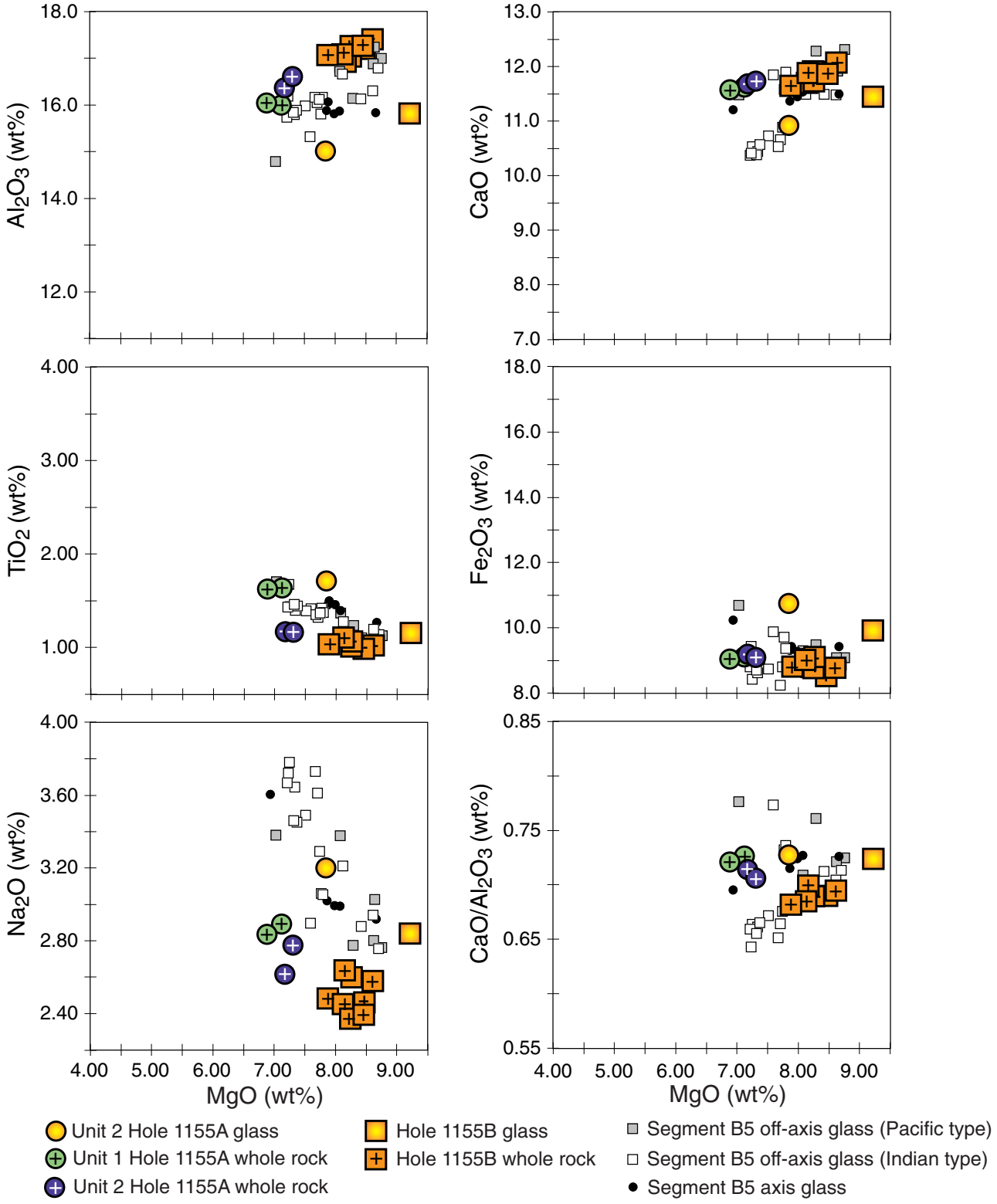

Figure F24. Trace element compositions vs. MgO for basalts from Holes 1155A and 1155B compared with Southeast Indian Ridge glasses from Segment B5. Symbols connected by lines show the analytical discrepancies between X-ray fluorescence and ICP-AES results where both techniques were used for the same powder.

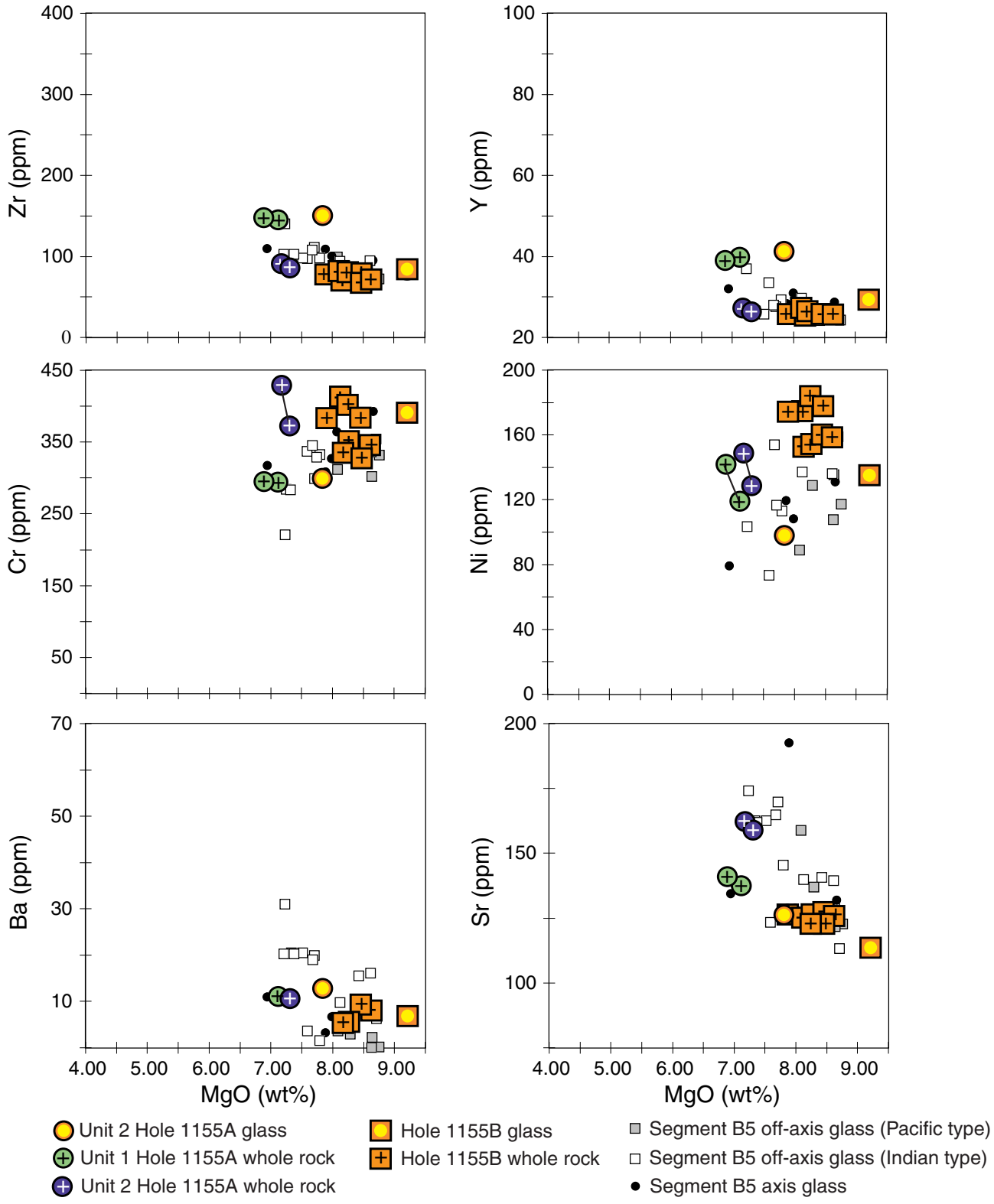

Figure F25. A. Variations of Zr/Ba vs. Ba for Hole 1155A and Hole 1155B basaltic glass and whole-rock samples compared with Indian- and Pacific-type mid-ocean-ridge basalt (MORB) fields defined by zero-age Southeast Indian Ridge (SEIR) lavas dredged between 123°E and 133°E. PRT = propagating rift tip lavas. **B.** Variations of Na_2O/TiO_2 vs. MgO for Hole 1155A and Hole 1155B basaltic glass and whole-rock samples compared with Indian- and Pacific-type MORB fields defined by zero-age SEIR lavas dredged between 123°E and 133°E. The dashed line separates Indian- and Pacific-type zero-age SEIR basalt glasses.

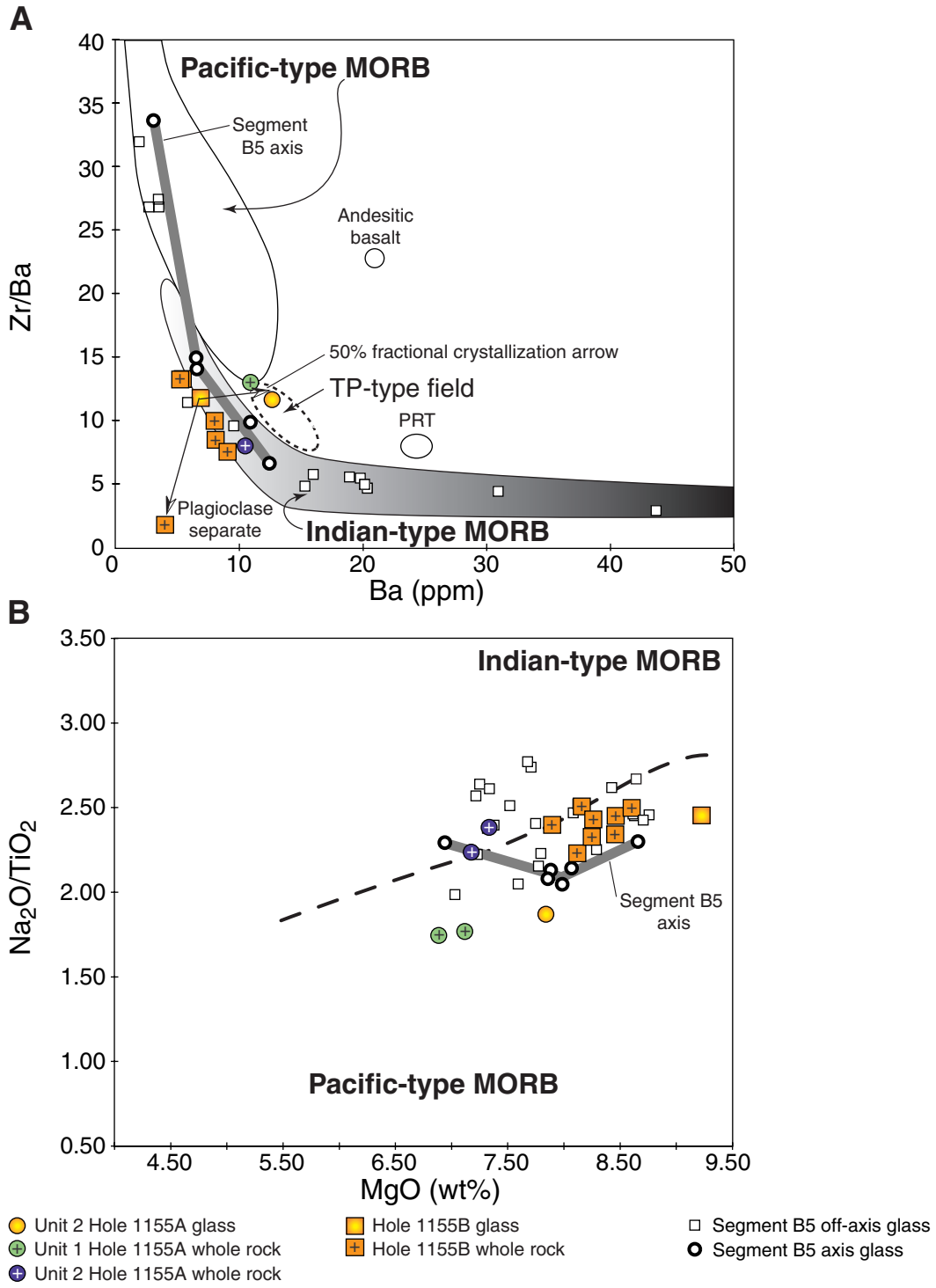

Table T1. Coring summary, Site 1155.

Hole 1155A
Latitude: 41°57.4925′S
Longitude: 127°59.6894′E
Time on hole: 1500 hr, 5 Dec 99–0300 hr, 7 Dec 99 (36.5 hr)
Time on site: 1500 hr, 5 Dec 99–0700 hr, 9 Dec 99 (88.0 hr)
Seafloor (drill-pipe measurement from rig floor, mbrf): 4986.4
Distance between rig floor and sea level (m): 11.0
Water depth (drill-pipe measurement from sea level, m): 4975.4
Total depth (from rig floor, mbrf): 5189.9
Total penetration (mbsf): 203.5
Total length of cored section (m): 26.2
Total length of drilled intervals (m): 177.3
Total core recovered (m): 2.34
Core recovery (%): 8.9
Total number of cores: 6
Total number of drilled cores: 1

Hole 1155B
Latitude: 41°57.4925′S
Longitude: 127°59.5417′E
Time on hole: 0300 hr, 7 Dec 99–0700 hr, 9 Dec 99 (51.5 hr)
Seafloor (drill-pipe measurement from rig floor, mbrf): 4986.4
Distance between rig floor and sea level (m): 11.0
Water depth (drill-pipe measurement from sea level, m): 4975.4
Total depth (from rig floor, mbrf): 5180.3
Total penetration (mbsf): 193.9
Total length of cored section (m): 46.0
Total length of drilled intervals (m): 147.9
Total core recovered (m): 18.18
Core recovery (%): 39.5
Total number of cores: 9
Total number of drilled cores: 1

Core	Date (Dec 1999)	Ship local time	Depth (mbsf) Top	Depth (mbsf) Bottom	Length (m) Cored	Length (m) Recovered	Recovery (%)	Comment
187-1155A-								
1W	6	0935	0.0	177.3	177.3	4.79	N/A	
2R	6	1200	177.3	180.8	3.5	0.69	19.7	Whirl-Pak
3R	6	1500	180.8	184.3	3.5	0.19	5.4	
4R	6	1810	184.3	188.9	4.6	0.28	6.1	
5R	6	2200	188.9	193.9	5.0	0.30	6.0	
6R	7	0015	193.9	198.5	4.6	0.23	5.0	
7R	7	0210	198.5	203.5	5.0	0.65	13.0	Whirl-Pak
				Cored:	26.2	2.34	8.9	
				Drilled:	177.3			
				Total:	203.5			
187-1155B-								
1W	7	1015	0.0	147.9	147.9	0.38	N/A	
2R	7	1200	147.9	151.5	3.6	1.39	38.6	Whirl-Pak
3R	7	1450	151.5	155.4	3.9	1.40	35.9	
4R	7	1925	155.4	160.1	4.7	1.87	39.8	
5R	7	2320	160.1	165.1	5.0	1.93	38.6	
6R	7	0330	165.1	169.7	4.6	3.81	82.8	
7R	8	0630	169.7	174.7	5.0	2.25	45.0	
8R	8	1025	174.7	179.4	4.7	3.45	73.4	
9R	8	1400	179.4	184.3	4.9	2.08	42.4	Whirl-Pak
10R	8	2000	184.3	193.9	9.6	0.00	0.0	Core catcher failed
				Cored:	46.0	18.18	39.5	
				Drilled:	147.9			
				Total:	193.9			

Notes: N/A = not applicable. This table is also available in ASCII format.

Table T2. Rock samples incubated for enrichment cultures and prepared for DNA analysis and electron microscope studies and microspheres evaluated for contamination.

			Enrichment cultures				DNA analysis			SEM/TEM samples		Microspheres†	
Core	Depth (mbsf)	Sample type	Anaerobic	Aerobic	Microcosm*	High pressure	Wash	Centrifuged	Fixed	Fixed	Air dried	Exterior	Interior
187-1155A-													
2R	177.3-180.8	Rock	10	3	1 Mn	X	X		X		X	Yes	No
187-1155B-													
2R	147.9-151.5	Rock	8	3	1 Fe/S	X	X		X	X	X	Yes	No
3R	151.5-155.4	Rock	10	3	1 Mn		X		X	X	X		
5R	160.1-165.1	Rock	8	3	1 Fe/S		X		X	X	X		
8R	174.7-179.4	Rock	9	3	1 Mn	X	X		X		X		
9R	179.4-184.3	Rock										Yes	No
		Seawater						X	X				

Notes: * = Microcosm for iron and sulfur (Fe/S) or manganese (Mn) redox cycles; SEM = scanning electron microscope; TEM = transmission electron microscopy; † = contamination test; X = sample prepared on board. This table is also available in **ASCII** format.

Table T3. Glass and whole-rock major and trace element compositions of basalts, Site 1155. (See table notes. Continued on next page.)

	Hole 1155A											Hole 1155B								
Core, section:	2R-1	2R-1	2R-1	2R-1	7R-1	7R-1	7R-1	7R-1	7R-1	5R-1	5R-1	2R-1	2R-1	2R-1	2R-1	2R-1	2R-1	2R-1	2R-1	2R-1
Interval (cm):	29-32	29-32	29-32	29-32	16-19	16-19	16-19	16-19	16-19	20-23	20-23	65-67	65-67	125-129	125-129	125-129	125-129	125-129	125-129	125-129
Depth (mbsf):	177.59	177.59	177.59	177.59	198.66	198.66	198.66	198.66	198.66	189.1	189.1	148.55	148.55	149.15	149.15	149.15	149.15	149.15	149.15	149.15
Piece:	7	7	7	7	3	3	3	3	3	4	4	7	7	15	15	15	15	15	15	15
Unit:	1	1	1	1	2	2	2	2	2	2	2	1	1	1	1	1	1	1	1	1
Analysis:	XRF	XRF	ICP	ICP	XRF	XRF	ICP	ICP	ICP	ICP	ICP	ICP	ICP	XRF	XRF	ICP	ICP	ICP	ICP	ICP
Rock type:	Sparsely to moderately plagioclase-olivine phyric basalt				Aphyric to sparsely olivine phyric basalt					Glass	Glass	Glass	Glass	Moderately plagioclase-olivine phyric basalt					Plagioclase	
Major element (wt%)																				
SiO_2	48.37	48.33	51.15	51.46	49.12	48.40	49.09	49.49	50.56	51.96	52.86	51.51	52.86	46.97	47.06	45.85	47.62	47.79	49.62	50.80
TiO_2	1.59	1.66	1.64	1.63	1.16	1.18	1.16	1.18	1.19	1.69	1.73	1.15	1.17	1.14	1.18	1.16	1.18	1.18	0.12	0.12
Al_2O_3	16.03	16.06	16.00	16.00	16.48	16.25	16.67	16.69	16.83	14.88	15.16	15.49	16.17	19.54	19.57	19.33	19.39	19.40	28.52	29.06
Fe_2O_3	9.02	9.08	9.09	9.14	9.28	9.12	9.07	9.18	9.27	11.05	10.45	10.05	9.79	9.90	9.97	9.79	9.90	9.86	1.37	1.40
MnO	0.14	0.15	0.15	0.15	0.14	0.14	0.14	0.15	0.15	0.18	0.18	0.17	0.17	0.13	0.14	0.14	0.14	0.14	0.05	0.05
MgO	6.89	6.88	7.16	7.08	7.23	7.12	7.30	7.32	7.47	8.01	7.67	9.37	9.07	2.97	2.97	3.21	3.21	3.22	0.98	1.02
CaO	11.56	11.58	11.61	11.64	11.80	11.57	11.64	11.83	12.04	10.81	11.04	11.20	11.69	12.90	12.90	12.79	12.88	12.88	16.18	16.23
Na_2O	2.84	2.83	2.78	3.00	2.68	2.55	2.68	2.90	2.83	3.15	3.25	2.69	3.00	2.88	2.83	2.81	2.95	2.99	2.70	2.91
K_2O	0.30	0.30	0.27	0.29	0.23	0.18	0.25	0.24	0.26	0.25	0.26	0.12	0.12	0.26	0.27	0.29	0.30	0.31	0.10	0.09
P_2O_5	0.20	0.20	0.22	0.22	0.12	0.17	0.14	0.14	0.14	0.22	0.23	0.12	0.13	0.18	0.18	0.19	0.20	0.20	0.03	0.03
LOI	1.18	1.18			1.64	1.64								1.42	1.42					
CO_2																				
H_2O																				
Total:	98.12	98.25	100.07	100.62	99.88	98.32	98.13	99.13	100.74	102.20	102.81	101.85	104.16	98.29	98.49	95.58	97.76	97.96	99.68	101.72
Trace element (ppm)																				
Nb	8				7									5						
Zr	148		143	147	91		86	85	88	149	152	82	84	85		80	82	82	7	7
Y	39		39	40	27		26	26	27	41	42	29	29	30		31	31	31	ND	ND
Sr	141		135	140	162		159	160	164	122	131	109	119	141		139	142	143	210	215
Rb	4				3									4						
Zn	86				75									85						
Cu	61				71									76						
Ni	142		118	120	149		129	130	130	99	97	135	135	118		103	108	103	38	35
Cr	295		300	290	429		369	376	380	301	298	403	380	446		343	353	356	45	47
V	262				245									273						
Ce	40				24									24						
Ba			11	11			10	11	11	12	13	7	7			8	8	8	4	4
Sc			35	35			35	35	36	37	36	37	37			38	38	38	11	11

Table T3 (continued).

	Hole 1155B																			
Core, section:	4R-2	4R-2	4R-2	4R-2	4R-2	6R-1	6R-1	6R-1	6R-1	6R-1	7R-1	7R-1	7R-1	7R-1	7R-1	9R-2	9R-2	9R-2	9R-2	9R-2
Interval (cm):	22-26	22-26	22-26	22-26	22-26	40-44	40-44	40-44	40-44	40-44	62-65	62-65	62-65	62-65	62-65	63-67	63-67	63-67	63-67	63-67
Depth (mbsf):	157.12	157.12	157.12	157.12	157.12	165.5	165.5	165.5	165.5	165.5	170.32	170.32	170.32	170.32	170.32	181.53	181.53	181.53	181.53	181.53
Piece:	5	5	5	5	5	4A	4A	4A	4A	4A	8B	8B	8B	8B	8B	8	8	8	8	8
Unit:	1	1	1	1	1	1	1	1	1	1	1	1	1	1	1	1	1	1	1	1
Analysis:	XRF	XRF	ICP	ICP	ICP	XRF	XRF	ICP	ICP	ICP	XRF	XRF	ICP	ICP	ICP	XRF	XRF	ICP	ICP	ICP
Rock type:	Moderately plagioclase-olivine phyric basalt					Moderately plagioclase-olivine phyric basalt					Moderately plagioclase-olivine phyric basalt					Moderately plagioclase-olivine phyric basalt				
Major element (wt%)																				
SiO_2	48.11	47.13	49.56	48.54	50.18	47.55	48.19	48.89	48.82	49.55	48.04	47.30	48.73	47.86	49.62	47.87	46.95	47.02	48.22	50.38
TiO_2	1.05	1.02	1.06	1.05	1.06	1.09	1.11	1.07	1.08	1.07	1.02	1.03	1.04	1.03	1.04	1.03	1.01	0.98	1.00	1.02
Al_2O_3	17.29	16.85	16.48	16.99	17.40	17.01	17.12	17.34	17.09	17.25	17.37	17.12	17.16	17.42	17.50	17.12	16.94	16.94	17.41	17.26
Fe_2O_3	8.78	8.92	8.83	8.79	8.71	9.03	9.14	9.04	9.16	9.13	8.86	8.65	8.73	8.80	8.83	8.80	8.64	8.35	8.57	8.80
MnO	0.15	0.14	0.16	0.15	0.15	0.16	0.16	0.15	0.15	0.16	0.14	0.15	0.15	0.15	0.15	0.14	0.14	0.14	0.15	0.15
MgO	7.98	7.82	8.16	8.14	8.18	8.05	8.20	8.09	8.32	8.37	8.51	8.40	8.58	8.56	8.67	8.39	8.11	8.35	8.49	8.53
CaO	11.78	11.50	11.82	11.87	11.91	11.65	11.76	11.99	11.74	11.93	11.99	11.80	11.99	11.96	12.23	11.81	11.65	11.66	11.86	12.08
Na_2O	2.50	2.47	2.68	2.55	2.68	2.39	2.51	2.63	2.59	2.59	2.45	2.35	2.60	2.56	2.59	2.39	2.36	2.28	2.56	2.53
K_2O	0.23	0.22	0.24	0.24	0.25	0.22	0.24	0.24	0.23	0.24	0.18	0.18	0.19	0.19	0.20	0.23	0.22	0.25	0.24	0.24
P_2O_5	0.10	0.09	0.11	0.11	0.11	0.10	0.10	0.12	0.12	0.12	0.10	0.10	0.11	0.12	0.12	0.09	0.09	0.12	0.11	0.11
LOI	1.13	1.13				1.02	1.02				0.65	0.65				0.54	0.54			
CO_2																				
H_2O																				
Total:	99.10	97.29	99.09	98.43	100.62	98.27	99.55	99.55	99.30	100.40	99.31	97.73	99.28	98.64	100.94	98.41	96.65	96.10	98.62	101.10
Trace element (ppm)																				
Nb	5					6					4					5				
Zr	78		71	73	72	80		74	73	76	77		70	73	70	78		70	71	70
Y	26		26	26	25	27		26	26	27	26		26	25	27	26		26	25	27
Sr	127		125	127	126	126		123	123	125	128		126	125	126	127		121	123	126
Rb	4					4					2					4				
Zn	67					69					64					65				
Cu	69					70					69					70				
Ni	175		153	151	156	174		152	154	156	177		161	153	161	184		157	159	164
Cr	383		349	324	331	412		357	343	353	384		358	336	344	401		312	325	348
V	220					238					222					232				
Ce	21					18					19					21				
Ba			5	5	6	87		6	6	6	85		8	8	8	84		9	10	10
Sc			33	33	33			35	34	34			33	32	33			33	33	33

Notes: LOI = loss on ignition; ND = none detected. This table is also available in **ASCII** format.